# FAILURE ANALYSIS OF ROTATING BAND UNDER RAMMED CONDITION FOR 155MM×52 CALIBER GUN SYSTEM THROUGH FINITE ELEMENT SIMULATIONS

**M.Tech. Thesis**

By

**PIYUSH PRADIP UPKARE**

**DISCIPLINE OF MECHANICAL ENGINEERING**

**INDIAN INSTITUTE OF TECHNOLOGY INDORE**

**JUNE 2023**

# FAILURE ANALYSIS OF ROTATING BAND UNDER RAMMED CONDITION FOR 155MM×52 CALIBER GUN SYSTEM THROUGH FINITE ELEMENT SIMULATIONS

**A THESIS**

*Submitted in partial fulfillment of the requirements for the award of the degree*

***of***

**Master of Technology**

*by*


**PIYUSH PRADIP UPKARE**



**DISCIPLINE OF MECHANICAL ENGINEERING**

**INDIAN INSTITUTE OF TECHNOLOGY INDORE**



**JUNE 2023**

# INDIAN INSTITUTE OF TECHNOLOGY INDORE

## CANDIDATE'S DECLARATION

I hereby certify that the work which is being presented in the thesis entitled **FAILURE ANALYSIS OF ROTATING BAND UNDER RAMMED CONDITION FOR 155MM × 52 CALIBER GUN SYSTEM THROUGH FINITE ELEMENT SIMULATIONS** in the partial fulfillment of the requirements for the award of the degree of **MASTER OF TECHNOLOGY** and submitted in the **DISCIPLINE OF MECHANICAL ENGINEERING, Indian Institute of Technology Indore**, is an authentic record of my own work carried out during the time period from August 2021 to June 2023 under the supervision **of Dr. Indrasen Singh**, Assistant Professor in Mechanical Engineering, Indian Institute of Technology Indore.

The matter presented in this thesis has not been submitted by me for the award of any other degree of this or any other institute.

06/06/2023

**Piyush Pradip Upkare**
**(M.Tech. Student)**

---

This is to certify that the above statement made by the candidate is correct to the best of my knowledge.

06/06/2023

**Dr. Indrasen Singh**
**(Thesis Supervisor)**

---

**Piyush Pradip Upkare** has successfully given his M.Tech. Oral Examination held on **25 May 2023**.

06/06/2023

Signature of Supervisor of M.Tech. thesis
Date: 06/06/2023

Satyanarayan

Convener, DPGC
Date: 07/06/23

Signature of PSPC Member 1
**(Dr. Ashish Rajak)**
Date: 06/06/2023

Signature of PSPC Member 2
**(Dr. Ram Sajeevan Maurya)**
Date: 06/06/2023

---

# ACKNOWLEDGEMENTS

I would like to express my sincere gratitude to my thesis supervisor **Dr. Indrasen Singh** for his valuable guidance and constant encouragement during my research work. Each and every discussion with him has always been educative and helped me to gained sound understanding, knowledge and awareness of scientific and technical aspect of my work. I am very thankful to him for teaching me how to analyze the results and how to write the research article. I am also thankful to my PSPC members: **Dr. Ashish Rajak** and **Dr. Ram Sajeevan Maurya,** for their continuous inputs and suggestions for this project.

I also want to thank **Mr. Sanjay Kumar**, Associate Director, **ARDE** for providing details of the given gun system as per requirement of simulation work and result validation. I appreciate his professional attitude, which allowed me to work with a clear mind and a free heart. I am thankful to **Mr. Sumit Chorma** and **all my lab mates** from Computational Solid Mechanics **(CSM) Lab**, IIT Indore for their unconditional help. Their excellence and knowledge in the field of Finite Element Simulation helped me a lot.

The entire **M.Tech. program** has been a valuable experience for me, not only in terms of acquiring skills in the fields of **Computational Mechanics, Finite Element analysis, System control and Design aspect**, but also in terms of learning a lot more about methods, research, work attitudes, and interpersonal relationships. I am thankful to all my friends from IIT Indore fore making this journey more enjoyable.

I would like to express heartfelt thanks to **my Parents and Sisters** for their blessings, efforts to maintain my morale and constant encouragement. Their love, support, and faith in me, always motivates me.

Finally, I am thankful to all those who assisted me in any way, whether directly or indirectly, during various stages of this work ……….. **Thank you everyone !!**

**Piyush Pradip Upkare**

(MTech in Mechanical Systems Design)

**Dedicated to**

**My Parents**

**Pradip Upkare & Lata Upkare**

# Abstract

The ballistic performance of artillery guns mainly depends on the interaction between rotating band and rifled barrel at the time of ramming and engraving process. This interaction is widely influenced by many important parameters such as ramming velocity, barrel wear and the geometry of rotating band. The experimental investigation on these parameters and their effect on ballistic performance is very costly and time consuming. However, the numerical analysis may provide insights on the deformation behavior. In the present work, artillery gun system with rifled barrel of 155 mm bore diameter is modeled in ABAQUS by developing a Python code. The explicit dynamic finite element (FE) simulations are performed to analyse the plastic deformation and failure of the rotating band.

The contact force, developed between rotating band and barrel, prevents the fallback of projectile at elevated angle and confirms the safety of ballistic operation. Thus, it is the most important parameter used to evaluate the ramming process. With this, a required ramming velocity for the worn barrels has been determined to provide a proper ramming condition and to meet the requirement of ramming operation throughout the life of the barrel. It is observed that the front portion of rotating band undergoes serve plastic deformation which indicates that engraving of front region of the band starts during ramming operation itself. These engraved profiles are then compared with experimental data provided by Armament Research & Development Establishment **(ARDE)**, a laboratory of Defence Research and Development Organisation **(DRDO)** and found reasonably comparable. Generally, a small angle of inclination is provided on the front region band to ensure smooth contact formation between band and barrel at the time of ramming. So, to analyze the effect of band geometry on ramming process, finite element simulations are performed by varying this inclination angle of the rotating band by half degree in the range of 1.5 ° to 3.5 °. Results obtained from these simulations depict that the

highest contact force is established if the inclination angle is equal to angle of forcing cone of the barrel.

Rotating band material offers high resistance, known as engraving resistance, while engraving. If band material doesn't find the space to flow, self-contact formation of band material takes place across the cannelure which further increases this engraving resistance. To avoid this situation, the suggestion of tapering of the cannelure is proposed. Results obtained after this modification indicate that overlap of band material is reduced and engraving of band took place much smoother. This reduces failure chances of rotating and ensures the performance of gun even after implementation of high propellant gas pressure.

# LIST OF PUBLICATIONS

**1.** Authors: Piyush P. Upkare, Sanjay Kumar and Indrasen Singh

Title: Analysis of ramming process for 155 mm caliber gun system.

(Manuscript under preparation)

**2.** Authors: Sanjay Kumar, Piyush P. Upkare, Sumit Chorma and Indrasen Singh

Title: Comparative study of engraving process of the rotating band into rifled barrel.

(Manuscript under preparation)

# TABLE OF CONTENTS

# LIST OF FIGURES

# LIST OF TABLES

# NOMENCLATURE

## Symbols :

| | |
|---|---|
| $R$ | Radius (mm) |
| $D$ | Diameter (mm) |
| $D_L$ | Land diameter of barrel rifling (mm) |
| $D_G$ | Groove diameter of barrel rifling (mm) |
| $W_L$ | Land width of barrel rifling (mm) |
| $W_G$ | Groove width of barrel rifling (mm) |
| $L_b$ | Total Barrel Length (mm) |
| $p_r$ | Pitch of barrel rifling (mm) |
| $V_r$ | Ramming Velocity (m/s) |
| $T$ | Time (s) |

## Greek letters :

| | |
|---|---|
| $\delta$ | Thickness of barrel rifling (mm) |
| $\theta$ | Helix angle of barrel riffling (degree) |
| $\mu$ | Coefficient of Friction |
| $\alpha$ | Inclination angle of front region of rotating band (degree) |

# ACRONYMS

| | |
|---|---|
| FEA | Finite Element Analysis |
| *DRDO* | Defence Research and Development Organization |
| ARDE | Armament Research and Development Establishment |
| C3D8R | Continuum 3-Dimensional 8 node linear brick element with reduced integration |
| JCCRT | Johnson-Cook Damage Initiation Criteria |
| PEEQ | Variable used in Abaqus for Plastic Equivalent Strain |
| CPRESS | Variable used in Abaqus for Contact Pressure |
| CNORMF | Variable used in Abaqus for Contact Force |

# Chapter 1

# Introduction

## 1.1. Overview: Description of Artillery guns

Artillery guns are heavy military weapons with long barrels used to launch munitions at long range. In the launching process, first burning of propellants takes place to build up gas pressure inside the chamber of gun which further becomes cause of motion of ammunition. The main components of artillery gun are shown in **Fig. 1.1** and briefly discussed below :

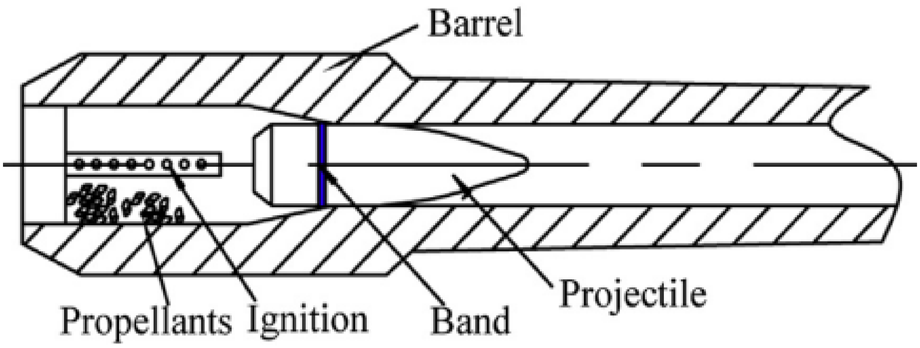


**Fig. 1.1:** Schematic of main components of artillery gun system.[1]

- Shell –
  Shell is a large caliber projectile fired by artillery. The payload of these projectiles is explosive or chemical filling which causes blast after hitting the goal. Fin less projectile gets aerodynamic stability by spinning about longitudinal axis. This spin is provided to the projectile by the interaction between rifling of gun barrel and rotating band.
- Barrel -
  It is a straight tube-like structure inside which projectile propels due to rapid expansion of high-pressure gases. For the given artillery gun system, the internal diameter (caliber) of barrel is 155 mm and the effective length of barrel is 52 times of caliber.

Generally rifling in the form of lands and grooves is provided to the barrel as shown in **Fig. 1.2.**

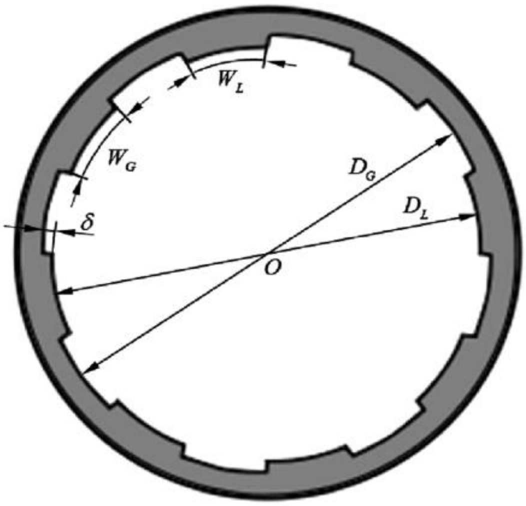


**Fig. 1.2:** Rifled barrel cross section [5]

- Rotating band –

  It is a band made up of soft material like gilding metal (CuZn10, alloy of copper and zinc). This band is placed near the base of projectile by pressing radially with a powerful hydraulic banding press.

## 1.2. Functional requirement of rotating band

The motion of the projectile inside the barrel is mainly governed by the interaction between rotating band and rifled barrel. Rotating band, also known as driving or slipping band, is like an extra material which is press fitted on the projectile and intend to perform some important functions stated as follows:

- Rotating band is responsible for positioning the projectile accurately inside the gun barrel. It centers the rear end of projectile and makes sure that it is concentric with barrel.
- The rotating band is designed such that the outer diameter of the band is slightly larger than the groove diameter of the barrel

which provides the interference fit and prevents the leakage of propellant gas.

- For the aerodynamic stability of finless projectiles spinning motion is necessary. The rotating band engages with the rifling of gun barrel and provides the required spin to the projectile while it is translating through the barrel.
- The interface configuration between the rotating band and barrel ensures no projectile falls back out of its seating at any angle of elevation.

While performing these functions, the rotating band should not exert excessive pressure on the barrel bore or on the walls of projectile. Also, it should reduce barrel wear as far as possible and perform satisfactorily in even badly worn-out guns.

## 1.3. Ramming Process

Ramming process is specifically for the positioning the projectile correctly inside the barrel by giving it initial velocity, called as initial ramming velocity. The positions of projectile at the beginning and the end of the ramming operation are displayed in the schematic shown in **Fig. 1.3(a)** and **(b)**, respectively.

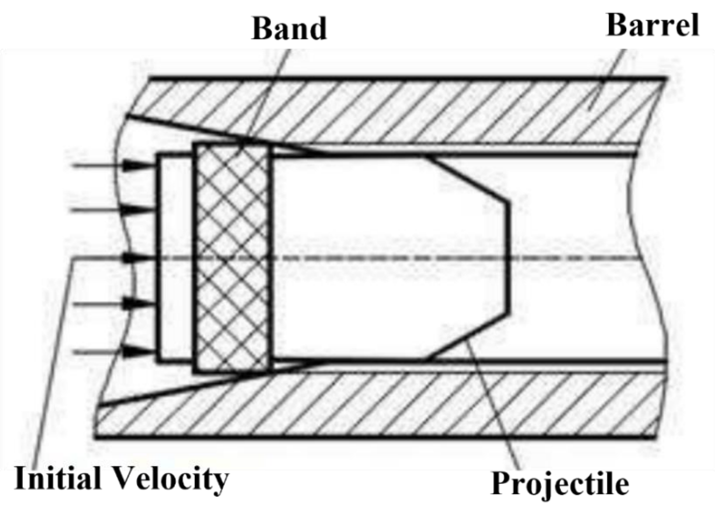


**Fig. 1.3 (a):** Positioning of projectile in barrel [12]

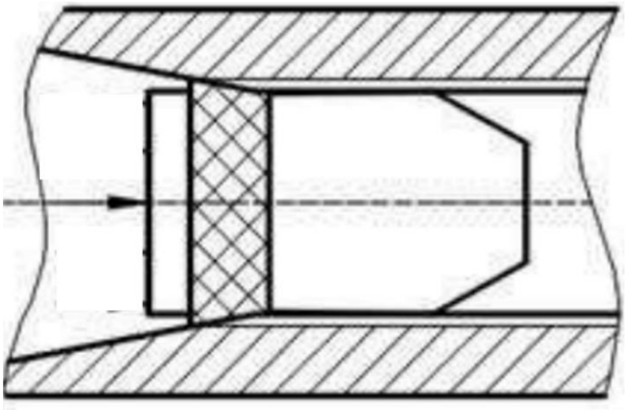

**Fig. 1.3 (b):** Projectile placed accurately inside the barrel. [12]

Generally ramming operation is performed manually known as hand ramming or with the help of some semi-actuating mechanism called as power ramming. In this process rotating band get compressed and fixed in the forcing cone of the barrel as shown in **Fig. 1.3 (b).** Once the ramming process is completed successfully, a check for safety is also done so that projectile should not fallback even if firing is to be done for elevated angle or firing weapon is moving rapidly over the bad road.

## 1.4. Engraving Process

After the ramming process is completed by fulfilling all safety requirements, the next task is to propel the projectile through the barrel. To obtain the motive force, propellants are burned in the barrel chamber which develops the high gas pressure and pushes the projectile in forward direction. As the projectile moves forward, the rotating band gets engraved due to the presence of rifling on the inner surface of barrel bore and imparts spinning motion to the projectile. **Fig. 1.4** depicts the schematic of engraving process.

As discussed earlier, for the aerodynamic stability of finless projectiles spinning motion is necessary which highlights the importance of engraving process. In this process of formation of land and grooves on the rotating band, it undergoes serve plastic deformation due to this there is possibility of failure of rotating band before the projectile propels outs of the barrel. If the band fails, many unavoidable phenomena like- leakage of propellant gas, yawing of projectile, barrel wear due to direct contact with projectile etc. will take which hampers the ballistic performance. So, to hit the target accurately and to achieve the desired range, the band should be in good condition throughout the engraving process.

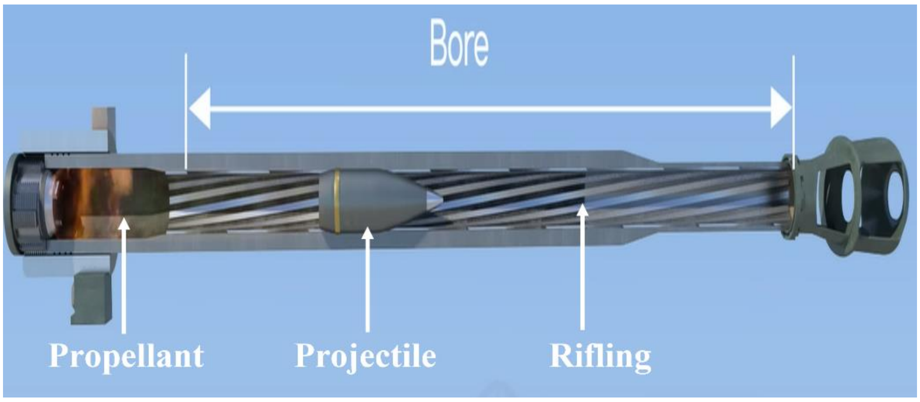


**Fig. 1.4:** Schematic of Engraving Process [2]

## 1.5. Thesis Organization

From the above discussion in above sections, it is clear that performance of artillery guns is greatly influenced by the ramming and engraving processes. The in-depth investigation of these processes is done in subsequent chapters of this thesis. The thesis comprises six chapters. The succeeding chapters are shortly described below to give a sound understanding about the contents covered in the thesis.

Chapter 2. **Literature review:** In this chapter, the pertinent literature is reviewed and the research gaps are highlighted. Further, the objectives of the thesis are also underlined.

Chapter 3. **Development of Finite Element Model:** Chapter 3 describes the development of 3D finite element model employed in the simulations of engraving operation.

**Chapter 4. Finite Element Simulation of Ramming Process:** In Chapter 4, the effects of ramming velocity, band wear and the initial geometry of rotating band of the ramming operations are investigated through finite element simulations. Results from simulation are validated with the experimental results.

**Chapter 5. Finite Element Simulation of engraving Process:** In this chapter explicit dynamic finite element simulations are performed to investigate the engraving process. Also, the possible design modifications for band design are provided to reduce the risk of band failure during engraving process.

**Chapter 6. Conclusion and Future Scope:** In Chapter 6, the accomplishment of objectives is examined. Significant findings are summarized, and the future scope of the study is suggested. for future studies are also briefed.

# Chapter 2

# Literature review

## 2.1 Introduction

In this chapter, the previous works pertaining to the deformation of rotating band and its interaction with the barrel are discussed. The important findings of these works are discussed in Section 2.2. Furthermore, substantial research gaps have been identified and listed as issues to be investigated in Section 2.3. Finally in Section 2.4, the objectives of the present study are underlined.

## 2.2 Review of pertinent Literature

The accurate position of the projectile in the bore of a barrel ensures the precise motion of a projectile after firing which results in reduced vibrations of projectile and wear of the barrel [3-6]. In the same process a check for safety is done so that projectile should not fallback even if firing is to be done for the highest possible elevated angle or fighting vehicle is moving rapidly over the bad terrain [7,8]. The force which is responsible for holding the projectile in the rammed, seated position is known as retention force. Balla et.al [11,12] have analyzed the ramming operation for howitzers and tank cannon, respectively. They concluded that in experimental conditions, measurement of retention force is difficult as rotating band experiences nonlinear elastic-plastic deformation during ramming operation. Therefore, the ejection force required to remove the projectile which has been correctly rammed earlier is measured and assumed to be equal as the retention force.

According to the criterion mentioned in the standard COS 109 002 [10], retention force of magnitude identical to the five times of the weight of projectile is suggested to be safe to prevent the potential dislodgement of the properly rammed projectile. Employing this criterion, Jankovych et al. [20] has discussed about the determination of ramming capability index ($C_{RD}$) and mentioned that ramming process is fully capable when $C_{RD}$ is equal to 3.86. Balla et al. and Prochazka et al. [14,15] have studied the thermos-plastic deformation of barrel chamber during ballistic process and concluded that barrel wear has intensive influence on the ramming process.

SUN et al. [16] implemented a combined constitutive model of plasticity and ductile damage for the penetration and contact problems based on continuum damage mechanics. In the model, the effect of strain, strain-rate and temperature has been considered. To analyze the stress fields Von Mises yield criterion, Johnson-Cook (JC) hardening model is applied. The model is implemented in the explicit dynamic finite element Abaqus workbench through the VUMAT subroutine. On the basis of JC model, the rotating band's engraving process is simulated, and the plastic deformation of band is studied. In addition, the effect of the stress state on damage evolution and the thermal softening effect is explained.

Andrews [17] has measured and investigated the strain caused by the high-pressure combustion products and the mechanical interactions between the rotating band and the rifling of the barrel, on the outer periphery of a barrel. Based on these measurements, he discussed the effect of rotating band pressure on the deformation of the walls of a barrel.

Sun et al. [18] has studied the effect of the rifling geometry on the interaction between an artillery Gun tube and an ammunition through finite element simulations of engraving process in commercially available software LS-Dyna. The results showed that the interior ballistic parameters such as the, the projectile advancement in barrel bore, muzzle velocity the resistance offered to the engraving and the engraving pressure varies significantly with the quantity of charge.

## 2.3 Research Gap

Although some understanding of ramming and engraving process is obtained by experimental and numerical analysis, there are several questions which remain unanswered. These are listed below:

- What will be the initial ramming velocity required for fully capable ramming of the gun barrel system with 155 mm rifled barrel bore?
- How does the ramming velocity changes with the increase in the wear of barrel?
- How and to what extent geometry of rotating band affects the ramming and engraving operation?
- What are the optimum values of material properties of rotating band to minimize the chances of failure in band even for enhanced chamber pressure?

## 2.4 Research Objectives

In order to address the above issues, the mechanism and mechanics of deformation of rotating band during ramming and engraving process needs to be well understood. To this end, the finite element simulations employing rate dependent plasticity models would help understanding the deformation behavior of band.

It must be mentioned that the retention force is mainly generated due to the reaction and frictional forces acting over the contacting surfaces of rotating band and barrel. Also, the portion of riffling in barrel over which ammunition gets placed at the end of ramming is minimal. Therefore, the effect of rifling on the ramming process could be ignored. On the other hand, a proper modelling of rifling must be incorporated for the analysis of failure in rotating band during engraving process.

In the view of this discussion, the following objectives have been defined for the present study:

- To develop the Finite Element model of artillery gun system consisting of projectile, rifled barrel and rotating band for the analysis of engraving process.
- To perform the finite element of simulations of engraving process by employing a rate dependent plasticity model.
- To perform finite element simulations of ramming process to understand the effect of ramming velocity and barrel wear on the retention force.
- To analyze the effect of band geometry on the ballistic performance.

# Chapter 3

# Development of Finite Element Model

## 3.1 Introduction

The 3D models of gun barrel, shell and rotating band are generated in commercially available software Abaqus 2017. The presence of riffling in the inner surface of barrel makes 3D modelling and meshing of barrel cumbersome and consumes a large amount of time. To avoid such problems, parametric modeling is employed to generate 3D model of barrel by writing a Python script readable by Abaqus which is discussed in Section 3.2. The details of the constitutive model which governs the deformation of rotating band are explained in Section 3.3. Finally, the details of the finite element mesh and contact definition employed in the simulations engraving process are highlighted in the Sec. 3.4 and 3.5, respectively.

## 3.2 Parametric modelling of barrel

A careful observation of a typical cross-section of barrel suggests that it can be created by rotation of a repetitive block comprised of a groove and land as depicted in **Fig. 3.1**. The repeating block ABCDEF in can be drawn by joining control points in space.

Let's the $r$ and $\beta$ represent coordinates of a control points with respect to a polar coordinate system with its origin at the center of chosen cross-section of barrel (refer **Fig. 3.1**). However, the coordinates of same control point with respect to a rectangular coordinate system are $X, Y$ and $Z$ which can be given by [1]:

$$X = r\cos\left(\frac{2\pi i}{M} + \beta\right) \tag{3.1}$$

$$Y = r \sin\left(\frac{2\pi i}{M} + \beta\right) \tag{3.2}$$

$$Z_i = \left(\frac{p_r}{M}\right) i = \left(\frac{2\pi R}{M \tan(\theta)}\right) i \tag{3.3}$$

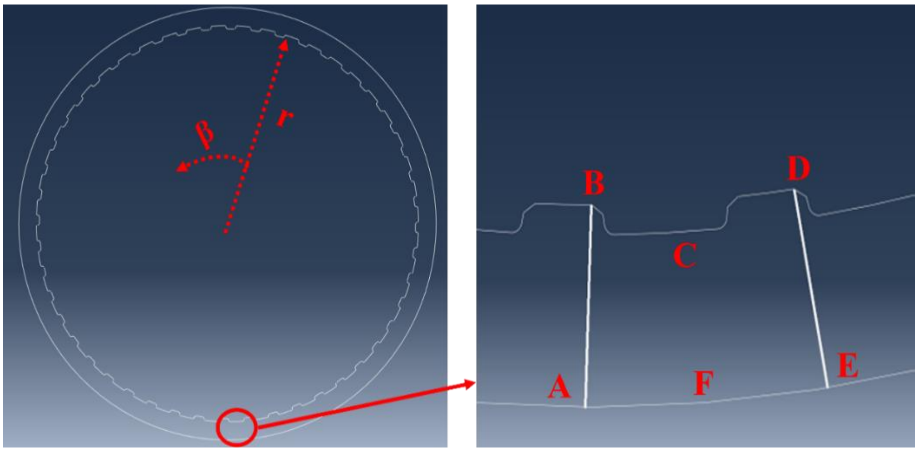


**Fig. 3.1.** A cross-section of gun barrel showing grooves and lands of riffling and the zoomed view of highlighted portion.

In these equations, $R$ is land-radius, and $i = 1, 2, 3, \dots L \times M$ is an index representing a typical cross section along the axis of barrel. Here, $L$ is a dimensionless parameter taken as the ratio of total barrel length, $L_b$ and pitch, $p_r$ of riffling which is defined as $p_r = \frac{2\,\pi\,R}{tan\,(\theta)}$ ($\theta$ being helix angle of riffling). Note that $Z_i$ represents the distance of $i^{th}$ repeating block from origin. Further, $M$ is a constant used to control the geometric accuracy of barrel. If M is 100, then there will be total 100 cross section, and the distance between two adjacent cross section will be $p_r/M$ mm.

To create repeating block, a total of thirteen control points has taken from the AutoCAD drawing provided by ARDE as shown in **Fig. 3.2**. It must be noted that control points 12 and 13 are the center of fillet used in the sketch. By substituting of the values $r$ and $\beta$ into the

**Eqs. 3.1-3.3**, the coordinates, $X$, $Y$ and $Z$ of the control points are determined and these points are marked in the ABAQUS sketch workbench with the use of Python Script. Further in **Fig. 3.3** the stepwise algorithm of this script is explained and the output of each step is shown in **Fig. 3.4.**

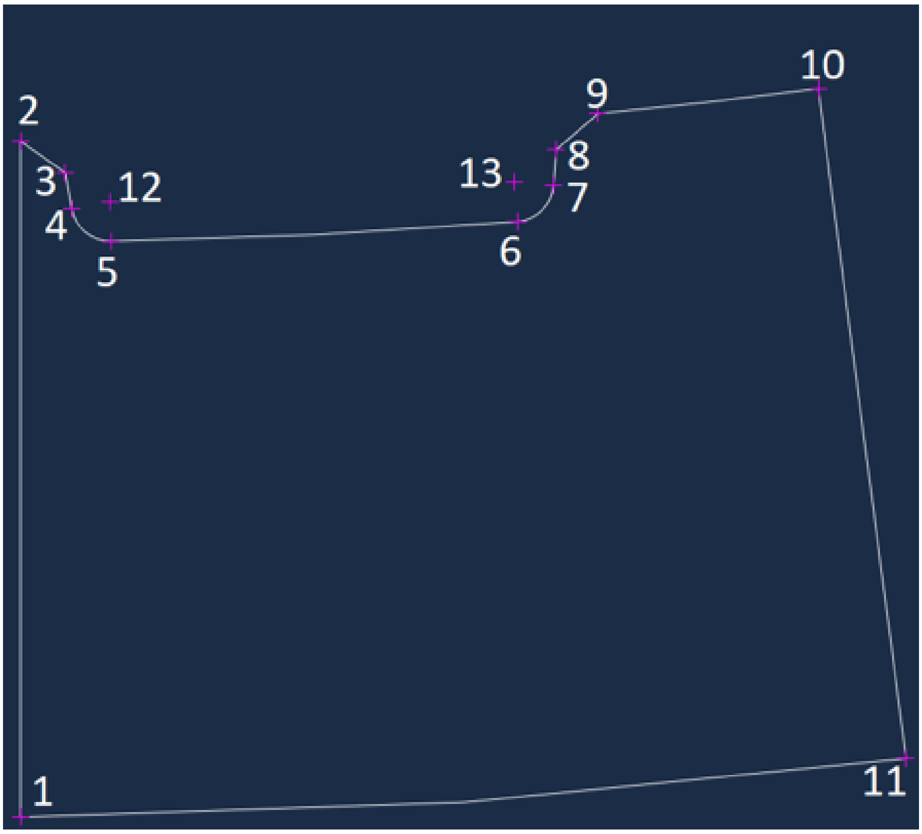


**Fig. 3.2**. Schematic of barrel rifling with thirteen control points used for Python script.

**Step (a)**

**Positioning the control points on ABAQUS sketch workbench, by converting polar coordinates into the cartesian coordinates**

**Step (b)**

**Joining the control points which are obtained in previous step with appropriate use of arcs and straight-lines which establishes wire profiles of the cross-section. The total number of wire profile obtained is $\boldsymbol{L \times M}$.**

**Step (c)**

**Call for the *Loft* command to develop a solid model with two adjacent wire profiles and repeat it for all. This step is required to run for $\boldsymbol{(L \times M) - 1}$ times.**

**Step (d)**

**Use of the *Circular Pattern* command to create N duplicate copies of the segmented solids and perform the *Boolean Union* operation. While performing *Union* operation boundaries of all instances are kept which further smoothens the generation of mesh.**

**Fig. 3.3** Flow chart of barrel modelling

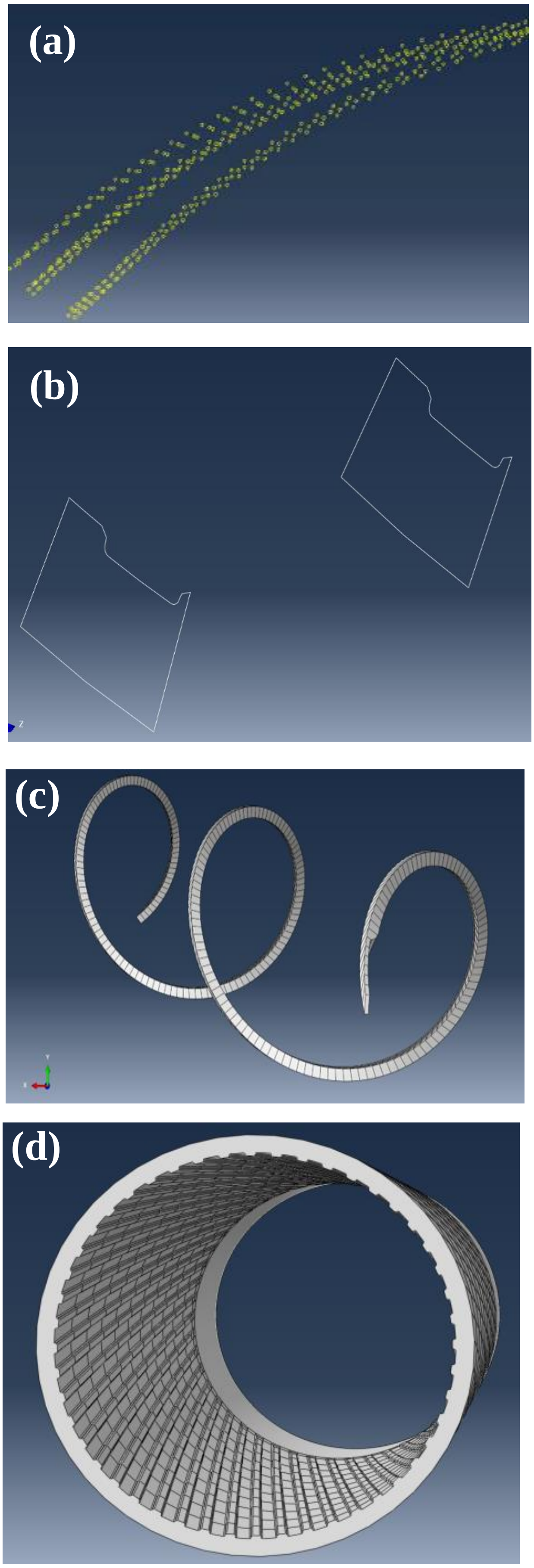


**Fig. 3.4**. Barrel modelling with joint use of Abaqus and Python Script

The dimensions required for the modelling of projectile and band are also provided by ARDE. So Finally, 3D models of projectile and rotating band are also created with the help of modelling commands already available in ABAQUS. Further the assembly of modeled component is done with appropriate position constraints. The section view of assembled 3D model is shown in **Fig. 3.5**

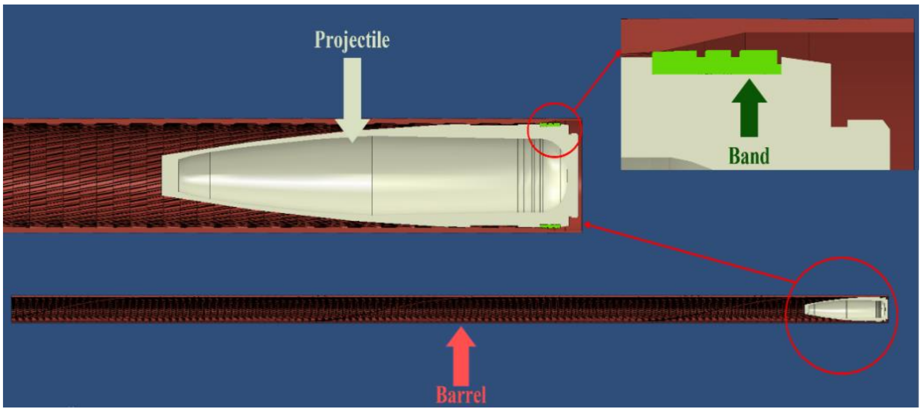


**Fig**. **3.5** Sectional zoomed view of 3D model of assembly of gun barrel system.

## 3.3 Constitutive Model

The plastic flow of the rotating band is assumed to follow the Johnson-Cook law to incorporate the effect of strain hardening and strain rate hardening. The stress-strain relationship followed by a typical ductile material is shown in **Fig. 3.6** [2]. It mainly consists of an elastic stage (O-A) and a plastic stage (A-D). The damage of the material initiates at point B, while the fracture of the material occurs at point D when the strain is large enough. The flow equation for this model is given below [2]:

$$\sigma_{eq} = [A + B\varepsilon_p^n] \times \left[1 + Cln\left(\frac{\dot{\varepsilon}_p}{\dot{\varepsilon}_0}\right)\right] \times \left[1 - \left(\frac{T - T_r}{T_m - T_r}\right)^m\right] \qquad (3.4)$$

Here, $\varepsilon_P$ is equivalent plastic strain, $\dot{\varepsilon}_{\mathrm{p}}$ is plastic strain rate, and $\dot{\varepsilon}_0$ is reference strain rate. Further, $T$ , $T_{\mathrm{r}}$ and $T_{\mathrm{m}}$ represent actual temperature, room temperature and melting temperature, respectively. Moreover, $\sigma_{\mathrm{eq}}$ is flow stress, while $A, B\ and\ C$ are yield strength of the material, work hardening coefficient and strain rate sensitivity respectively. Further, the constants $n$ and $m$ in Eq. 3.4 represent work hardening exponent and thermal softening coefficient, respectively.

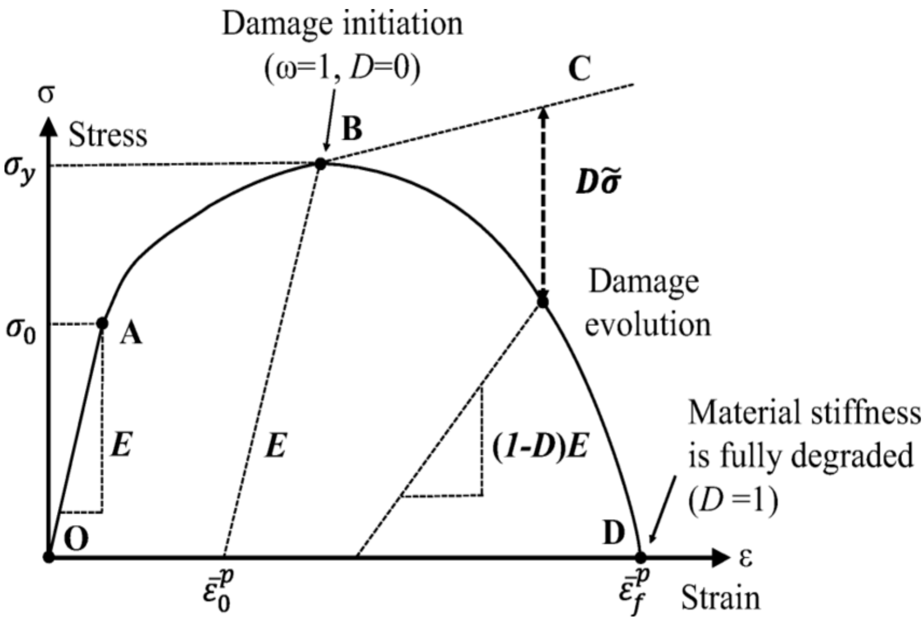


**Fig. 3.6**. Material constitutive for the rotating band [2]

To simulate the failure in the rotating band during ramming, the damage model of Johnson-Cook, which is given by **Eq. 3.5** is employed [2].

$$\bar{\varepsilon}_f^p = [D_1 + D_2 exp\,(-D_3\,\eta)] \times \left[1 + D_4 ln\left(\frac{\dot{\varepsilon}_p}{\dot{\varepsilon}_0}\right)\right] \times \left[1 + D_5\left(\frac{T - T_r}{T_m - T_r}\right)\right] \tag{3.5}$$

In **Eq. 3.5**, $D_1 - D_5$ are damage parameters, while $\bar{\varepsilon}_{\mathrm{f}}^p$ is equivalent failure strain. Further, $\eta = \frac{\sigma_H}{\sigma_{eq}}$ is stress triaxiality where $\sigma_H$ is hydrostatic stress.

The damage in material is assumed to commence when the state variable ω becomes unity as indicated by *Point B* in **Fig. 3.6.** The definition of ω is mentioned in **Eq. 3.6** [19].

$$\omega = \int \frac{d\epsilon^p}{\bar{\varepsilon}_f^p(\eta, \dot{\epsilon^p})} \tag{3.6}$$

After onset of damage, the stiffness, $\sigma$, of failing element is assumed to degrade as:

$$\sigma = (1 - D)\sigma_{eq}, \tag{3.7}$$

Where $D$ is damage parameter which evolves from zero to unity as:

$$\dot{D} = \frac{L_{eq}\,\dot{\varepsilon}^p}{\bar{u}_f^p} \tag{3.8}$$

In **Eq. 3.8**, $L_{eq}$ is the characteristic length of the element while $\bar{u}_f^p$ is the effective plastic displacement at full degradation/failure.

Rotating band is made up of gilding metal, an alloy of copper and zinc. By varying the proportions of copper and zinc, the properties of this alloy (brass) can be changed, allowing hard and soft brasses. Generally, the gilding metal with 10% zinc is most popular in the defense sector. On the other hand, barrel and projectile are made up of high strength materials like steel. The Young's modulus, Poisson's ratio and density of these materials are provided in the **Table. 3.1** [3]**.** The material of band is assumed to follow the Johnson-Cook material model as discussed above. The values of material constants appearing in this model are taken from [3] and listed in **Table. 3.2.**

**Table. 3.1** Mechanical Properties of the materials used in model.[3]

| Part name | Material | Young's modulus, E (GPa) | Poisson's ratio, ε | Density, ρ (kg m−3) |
|---|---|---|---|---|
| Rotating band | CuZn10 | 121 | 0.33 | 8944 |
| Projectile and barrel | Steel | 207 | 0.29 | 7850 |

**Table. 3.2** The Johnson-Cook (J-C) parameters for rotating band [3]

| Parameter | Value | Parameter | Value |
|---|---|---|---|
| **A (MPa)** | 90 | **D1** | 0.54 |
| **B (MPa)** | 292 | **D2** | 4.89 |
| **C** | 0.025 | **D3** | 3.03 |
| **N** | 0.31 | **D4** | 0.014 |
| **M** | 1.09 | **D5** | 1.12 |

## 3.4 Mesh generation strategy

As the dimensions of some components in given gun system are very large compared to others, the meshing should be done very wisely. Large number of mesh elements increases the computational time and consumes more resources, so the identification of regions which plays vital role in the numerical analysis is important. In the discretization, Continuum 3-Dimensional 8 node linear brick element with reduced integration (C3D8R) is used. To enhance stability and efficiency of calculations option like distortion control and stiffness hourglass control are enabled. The rotating band is the main focus of this failure analysis, and it undergoes severe plastic deformation in ballistic process. In order to capture the large strain and stress gradient, a highly refined mesh with smallest element size of 0.3 mm is employed to discretise the rotating band and barrel rifling near the forcing cone. Also, the region in the projectile which is in the contact with band are discretised with finer elements, while remaining portion of barrel and projectile are discretised by coarser elements to reduce computational time. In case of band, special care is taken to have helical mesh with angle equal to the helix angle (θ) of rifling in barrel. The finite element mesh of projectile, barrel and rotating band is shown in **Fig. 3.7-3.9,** respectively.

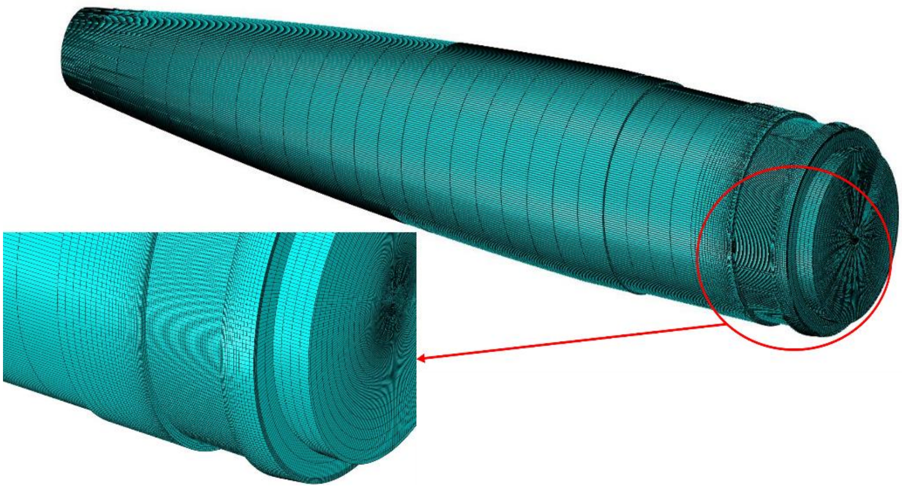

**Fig. 3.7**. Meshed model of projectile.

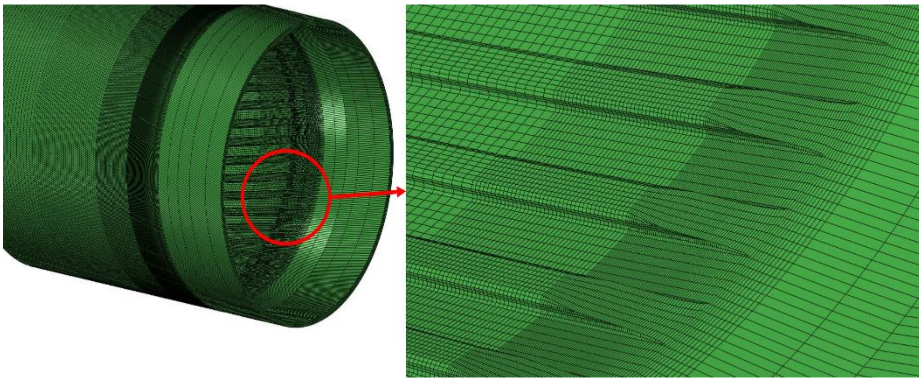

**Fig. 3.8**. Meshed model of rifled barrel

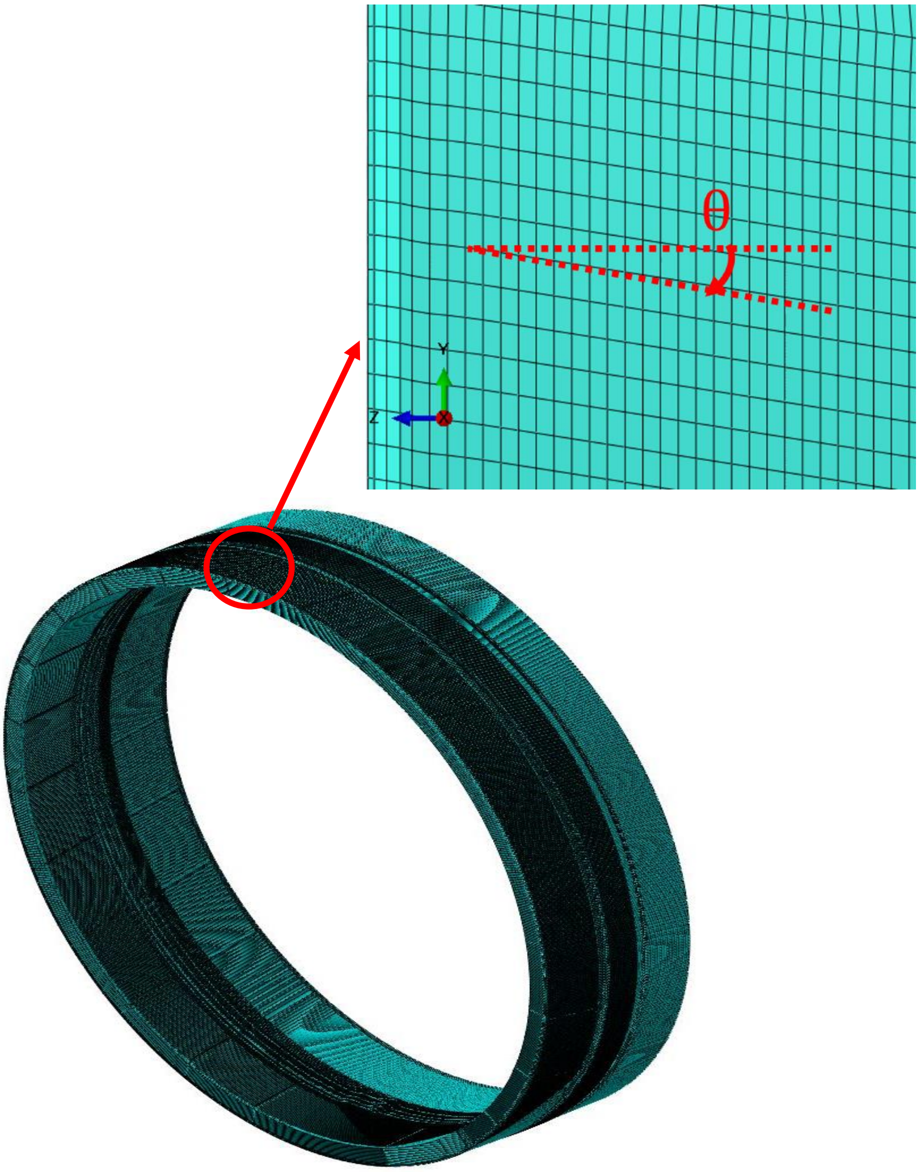


**Fig. 3.9**. Helically meshed rotating band with angle equal to the helix angle (θ) of rifling in barrel.

## 3.5 Contact Definition

A general contact (Explicit) algorithm inbuild with Abaqus is used to model interaction between barrel and band as well as band and projectile. Further, normal and tangential behaviour are characterised by assuming coefficient of friction between meeting surfaces as 0.1. It must be noted that the internal element-surfaces of the rotating band are also defined to ensure contact is established between the barrel and newly created surface on band after deletion of failed element in the band. In addition, the tie constraint is applied to restrict the slipping between projectile and band during deformation. To remove the failed element from the model, STATUS option available with the Abaqus is kept activated in all the simulations.

# Chapter 4

# Finite Element Simulation of Ramming Process

## 4.1 Introduction

Ramming is specifically done for the positioning the projectile correctly inside the barrel by giving it initial velocity, called as initial ramming velocity. Ramming can be a hand ramming which is performed manually, or a power ramming if performed with the help of some semi-actuating mechanism. This chapter deals with the numerical analysis of ramming process. Simulation details of are given in Section 4.2. Further, the results obtained from these simulations are validated with experimental results provided by ARDE, as discussed in Section 4.3.

## 4.2 The Modelling strategies

In chapter 3, the modelling and meshing part for artillery gun barrel system has already been discussed. By understanding the main features of ramming process carefully, following assumptions are made to simplify the numerical calculations for more efficient simulation:

- The influence of helix angle of barrel rifling is ignored as the projectile travels very less distance inside the forcing cone during ramming operation.
- The cross-section of the barrel is symmetrical even after it worn, that is wearing of barrel is assumed to be uniform and axisymmetric.
- Thermal effects are neglected for all simulations.

Considering the assumptions stated above, a ramming process can be simulated by modelling only a portion of a barrel and ammunition employing axisymmetric conditions. Thus, the analysis of ramming process is performed by modelling only a 15-degree sector-section of complete model which correspondence to the two grooves and two lands. To reduce total number of elements in simulation, instead of modelling full length barrel only forcing cone portion of barrel is taken for analysis. Assembly of gun barrel system particular for the ramming process is depicted in **Fig. 4.1.**

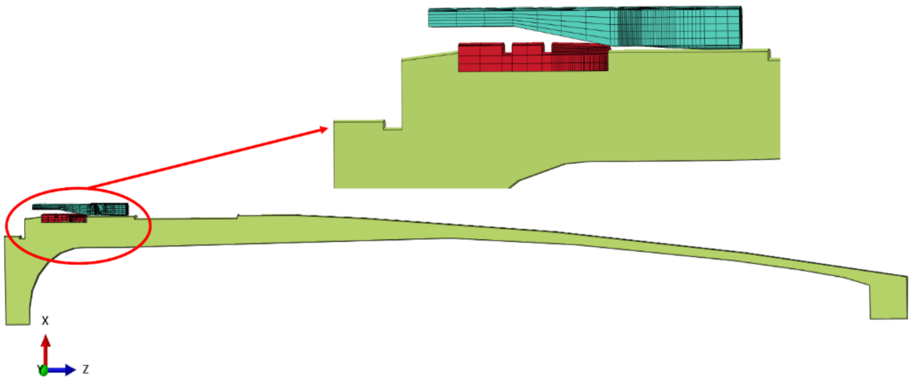

**Fig. 4.1:** 15-degree section of full 3D model with modified band mesh used for ramming analysis.

Further, the load and boundary conditions employed in the analysis of ramming process are depicted in the schematic shown in **Fig. 4.2.** The simulation of ramming process is consists of two analysis steps. In the first step, initial ramming velocity is given to the projectile which can move only in axial (Z) direction. All the nodal degrees of freedom are restricted for the one face of barrel which fixes barrel in one position. The elements corresponding to the side faces of band and barrel are constraint to move in angular ($\theta$ ) direction. The gravity load is applied in terms of axial and radial components which takes care of effect of angle of inclination for ramming process. The duration of step 1 is kept sufficiently longer for projectile get stopped inside the barrel.

In the second step, pressure equivalent to five times of the weight of projectile is applied on the front face of projectile to check if contact force generated between band and barrel is sufficient to prevent the fallback of projectile.

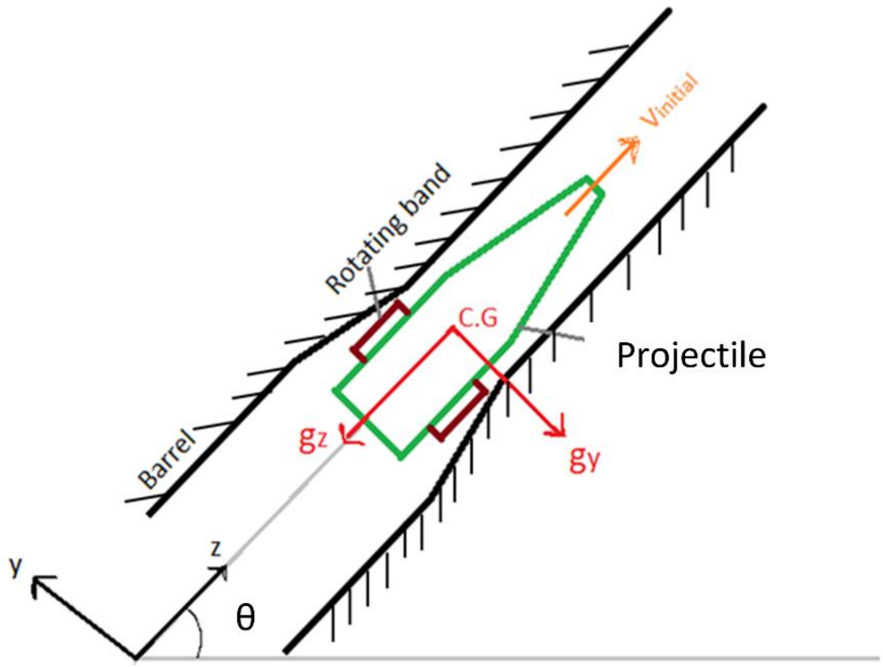


**Fig. 4.2:** Schematic of load and boundary condition for ramming process

## 4.3 Results and discussion

### 4.3.1 Analysis with New Barrel

The key results from the simulations of ramming process for new barrel are discussed in this section. **Fig. 4.3** shows the variation of contact force between rotating band and barrel inner surface and velocity of projectile with time. The impact of band on inner surface of barrel and their further interaction is a non-linear dynamic process due to which oscillating variation is observed in velocity and force profile. This typical behavior is identified as ping-pong effect [9]. It should be noted that $point\ a$ on velocity curve and $point\ a'$ on contact force curve corresponds to same time instant $t = 0.933\ ms$, similarly $point\ b$ and $b'$ corresponds to same time instant $t = 2.53\ ms$.

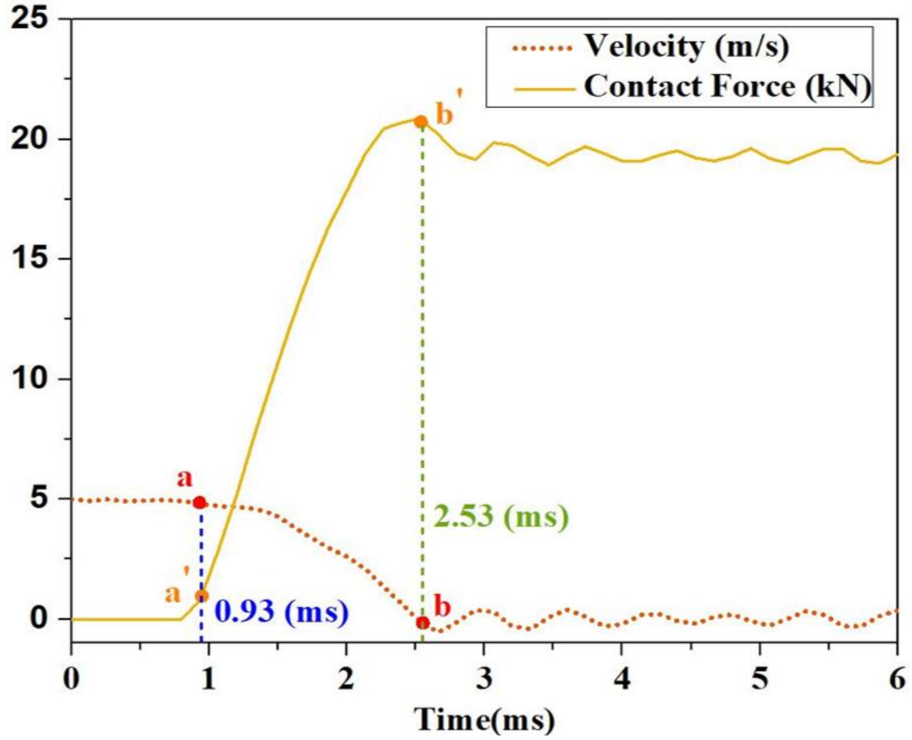


**Fig. 4.3:** Evolution of ramming velocity and contact force with time

It can be seen that the velocity of the projectile remains almost identical to the initial velocity of 5 m/s up to $point\ a$ and begins to drop rapidly thereafter. It is important to observe from the curve pertaining to the contact force that the contact force begins to evolve at around same time suggesting rotating band starts contacting the barrel at $t = 0.933\ ms$. The contact force further increases with the reduction in diameter of forcing cone, consequently the projectile velocity continues to drop and become almost zero at around $point\ b$.

**Fig. 4.4** indicates the displacement-time profile for projectile motion. $Point\ a$ and $b$ corresponds to stages identical to the that marked in Fig. 4.3. Note, the projectile has travelled near to 4.5 mm to establish contact between rotating band and barrel $(point\ a)$. Completion of ramming process is indicated by $point\ b$, which corresponds to maximum projectile displacement. After this point there is no change in displacement profile which shows that projectile is successfully positioned inside the barrel. *Point c* corresponds to the start of step 2, in which extraction force is applied on front surface of projectile. As there is no change in displacement value, it can be concluded that frictional contact force induced between band and barrel is sufficient enough to prevent the fallback of projectile even when extraction force equal to the 5 times of the projectile weight. Thus, safety in the process is ensured and the main goal of ramming is achieved.

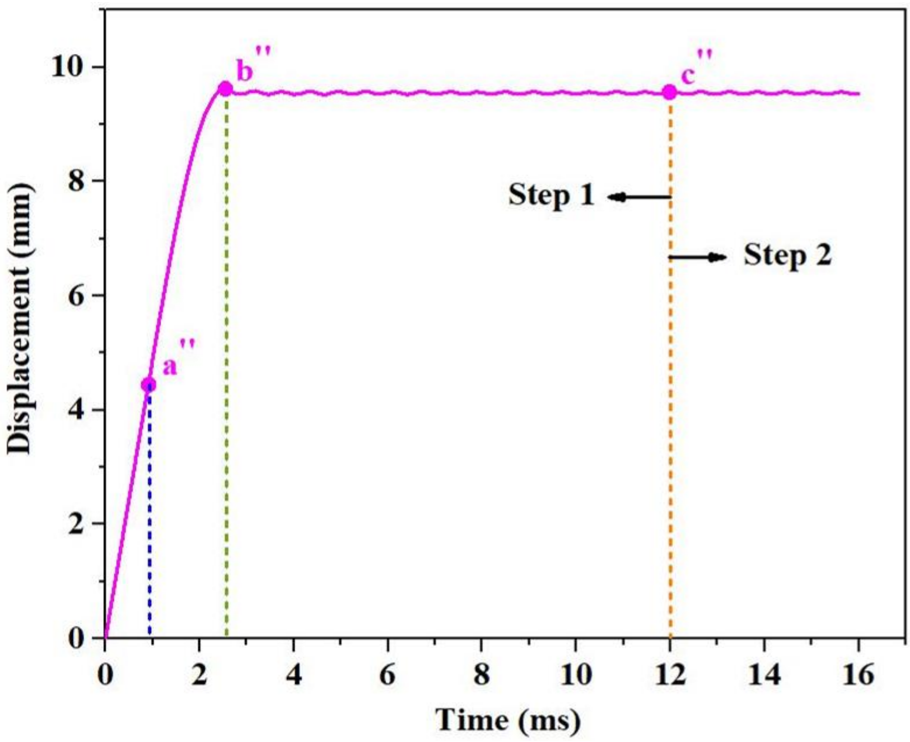


**Fig. 4.4:** Axial displacement of projectile

It can be depicted from **Fig. 4.5 (a)** that engraving of band has started during the ramming process itself. A significant plastic deformation has taken place in the front region of the rotating band. The CPRESS parameter gives the value of contact pressure on the surface of rotating band. The shape and size of this region is very similar to the shape and sizes of lands at the beginning of riffling. The length of the grooves on the engraved band is 7 mm which is compatible with the experimental result shown in **Fig. 4.3 (b).**

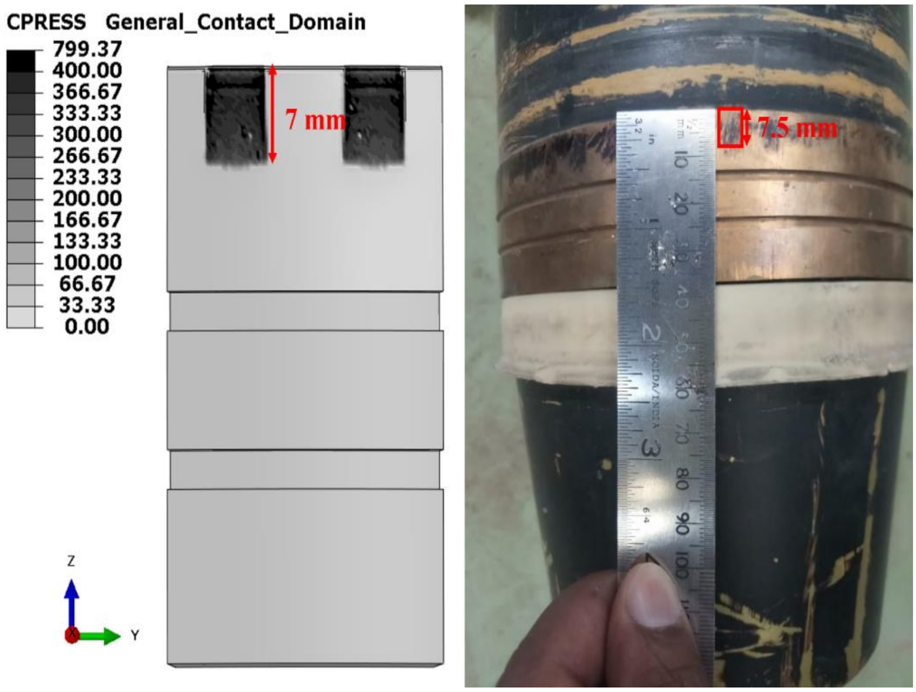


**Fig. 4.5**. (a) Contact pressure contours indicating start of engraving during ramming process. (b) Experimental result [DRDO]

### 4.3.2 Analysis with Worn Barrel

Similar sets of simulation are performed to study the effect of barrel wear on the contact force between barrel and band. **Fig. 4.6** shows the evolution of contact force corresponding to four barrels having different wear percentages. Percentage wear is the increase in the land diameter with respect to original diameter. Contact force profile for new barrel is also shown again for comparison. Thus, it is observed that with increase in barrel wear the magnitude of contact force between rotating band and barrel continues to decrease.

Points marked on respective profile give the time instant at which contact between barrel and band surfaces initiates. At these instants displacement of projectile is noted from respective displacement verses time curve and tabulated in the table below. **Table. 4.1** reveals that as the wear in barrel increases, projectile must travel more and more distance to establish contact between band and barrel. Thus, the formation of contact is delayed.

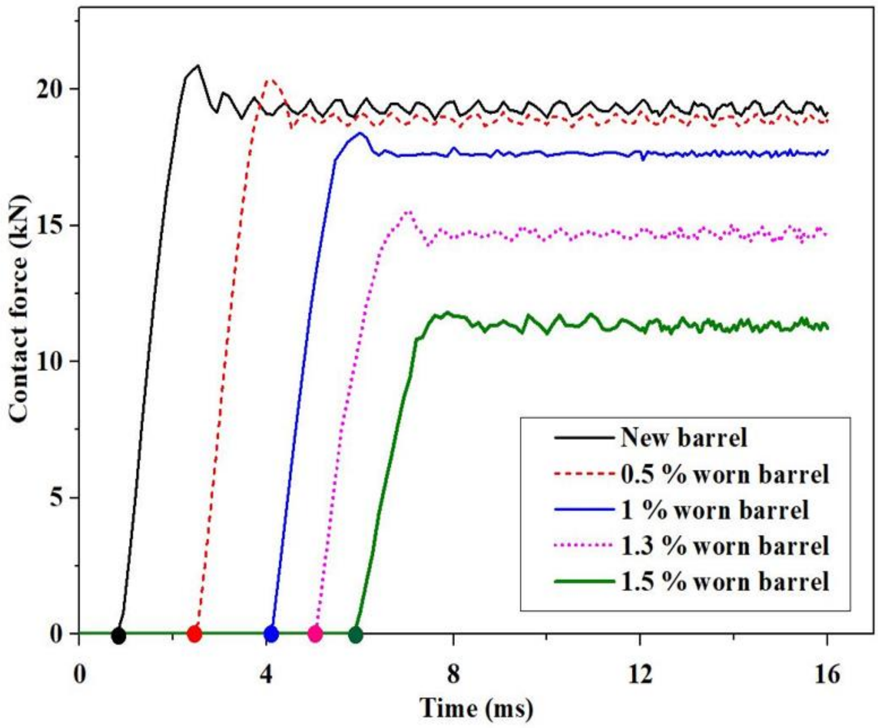


**Fig. 4.6** Contact force variation for new and worn barrels under same ramming condition.

**Table. 4.1** Contact initiation for each type of barrel.

| Barrel Type | Time instant of contact initiation (ms) | Projectile displacement at that instant (mm) |
|---|---|---|
| **New Barrel** | 0.93 | 4.57 |
| **0.5 % worn** | 2.53 | 12.37 |
| **1 % worn** | 4.13 | 20.16 |
| **1.3 % worn** | 5.06 | 24.7 |
| **1.5 % worn** | 6 | 29.2 |

To have proper comparison, the normalized contact force, $CF_{norm}$, defined as the ratio of the maximum contact force in a worn barrel and the maximum contact force in a new barrel, is recorded. Then variation of $CF_{norm}$ against the land diameter, $D_{land}$ is shown in **Fig. 4.7. This figure** shows that rate of decrease in contact force is near to ten percent for the initial wearing conditions barrels (0.5 % and 1% worn barrel). But this decrement increases very rapidly as more and more wear of barrel takes place. If we correlate the barrel wear with number of shots fired, then one can easily predict the working life of the barrel.

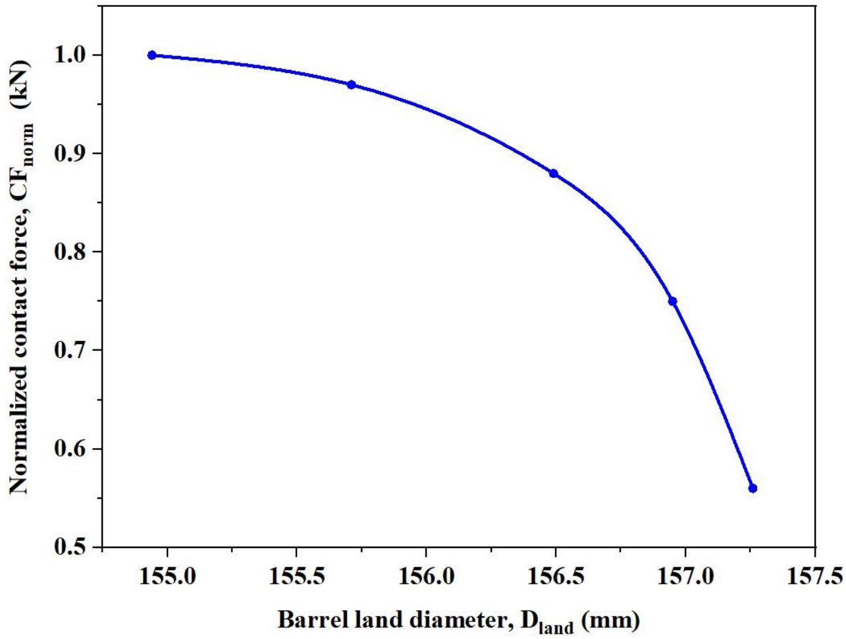


**Fig. 4.7** Variation in normalized contact force

Even though the forcing cone dimensions are changed due to wear, the weight of the projectile will be the same for all future firings. So, it is required that worn out barrels should also provide the same magnitude of contact force as by new barrel. This is a necessary condition to keep the worn barrel in working condition. To fulfill this requirement, one option is to ram the projectile with higher ramming velocity ($V_r$). So, another set of simulations are performed to find out the ramming velocity required to achieve the contact force in a worn-out barrel identical to that applied by new barrel. Note that for each barrel to get the contact force equal to the reference contact force of 20 kN (Contact force corresponding to the new barrel). **Fig. 4.8** depicts that as the wear of barrel increases, projectile should be rammed by more velocity. For example, the initial ramming velocity of projectile should be increased to 11.7 m/s when it has to fire in the barrel whose inner bore has undergone a wear of 1.5 percentage. By considering ramming velocities values for five types of barrels, variation in $V_r$ with barrel land diameter is plotted in **Fig. 4.9**. With the help of this graph and by doing interpolation, required ramming velocity can be determined for the any type of worn barrel which has undergone wear up to 1.5 percentage.

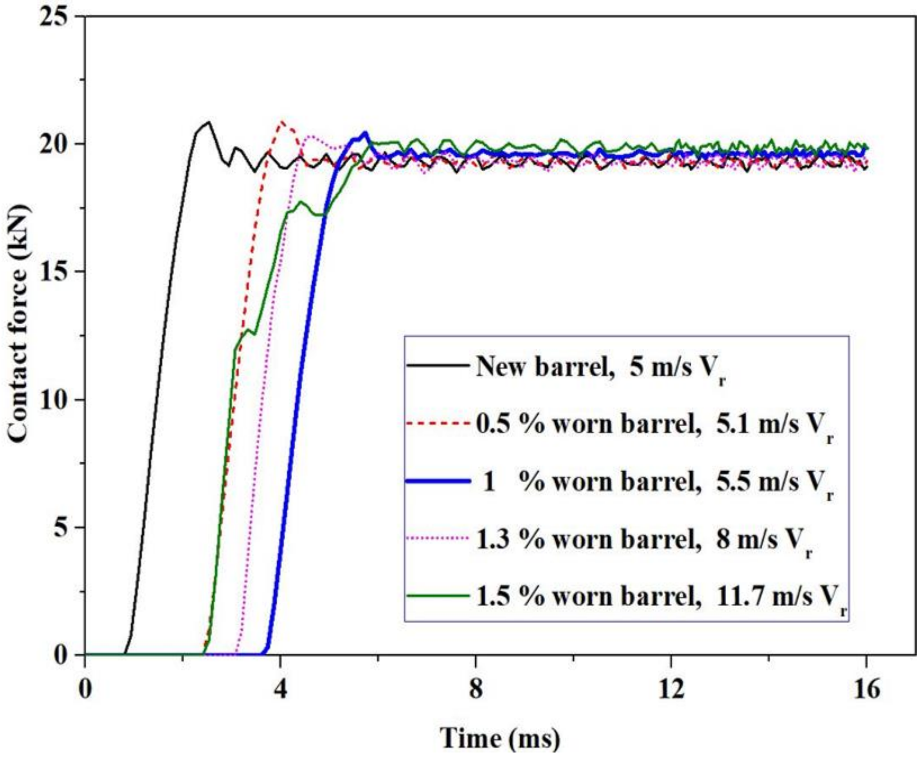


**Fig. 4.8** Required ramming velocity ($V_r$) for worn-out barrels to develop reference contact force.

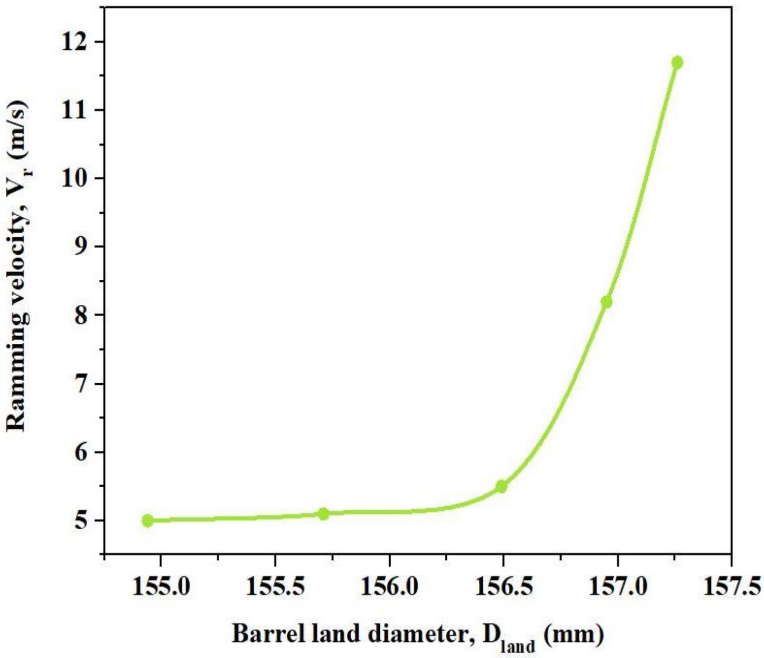


**Fig. 4.9.** Variation in initial ramming velocity for worn out barrels.

### 4.3.3 Effect of band geometry

The geometry of the band is expected to considerably influence the contact force. Since the ramming process is primarily governed by contact force, the effect of band geometry on the contact force needs to be analyzed. The one vital parameter from band geometry which governs this interaction is inclination angle of leading surface of band. Therefore, the FE analysis of ramming process is performed by varying this angle from 1.5 ° to 3.5 °. **Fig. 4.10** shows variation in contact force for the five rotating bands with different front inclination angles. It is observed that contact force increases with inclination angle, attains a peak for the band with inclination of $3^o$, and decreases again with further increase in inclination.

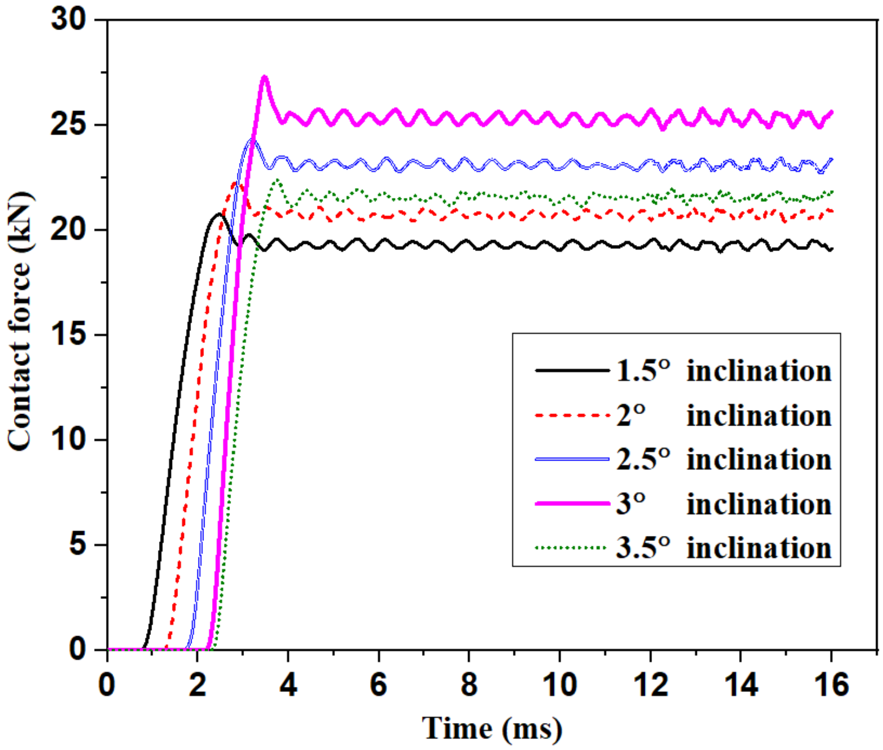


**Fig. 4.10.** Development of contact force for the bands with different angle of inclination of leading surface.

To understand the mechanics behind this variation, detailed analysis is done for bands with α values of 1.5 °, 3° and 3.5 °. As contact force mainly depends on the contact pressure and contact area , it is desirable to study these two factors individually. Initially the evolution of band pressure along axial direction is observed and pressure values are extracted for the path starting from *p* and ending on *q* as shown in **Fig. 4.11**. From the graph obtained it can be depicted that, for case *c* pressure continues to increase from point *p* attains peak at the midway of path and finally falls down as point *q* approaches. On the other hand, exactly opposite trend is observed for *case a*. While in *case b*, there is gradual increase in pressure starting from point *p* and values remain significant on complete path length.

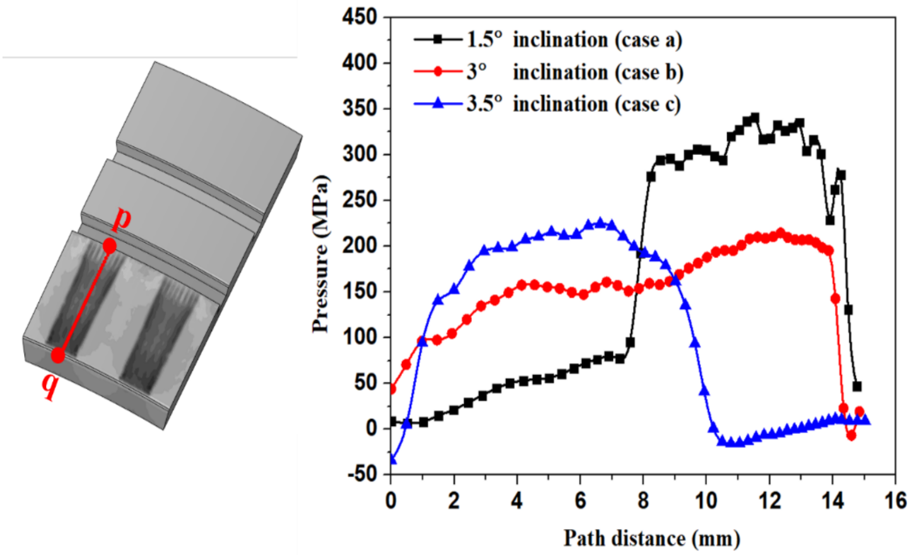


**Fig. 4.11.** Comparison of band pressure for three types of bands.

Before examining the second factor which is contact area, it should be noted that the extent of plastic deformation and portion of rotating band which experiences this deformation is different for each case. The sectional view of band and barrel after the formation of contact is shown in **Fig. 4.12**. The parameter PEEQ represents equivalent plastic strain in the deform model. For *case a*, plastic deformation takes place at the very front portion of band and this deformation zone shifts backward as the value of α increases (*case b* and *case c* ). The extent of deformation is also high in *case a*, as there is more band material which undergoes compression as projectile advances inside the forcing cone of barrel, which is in accordance with sudden hike in pressure curve seen earlier.

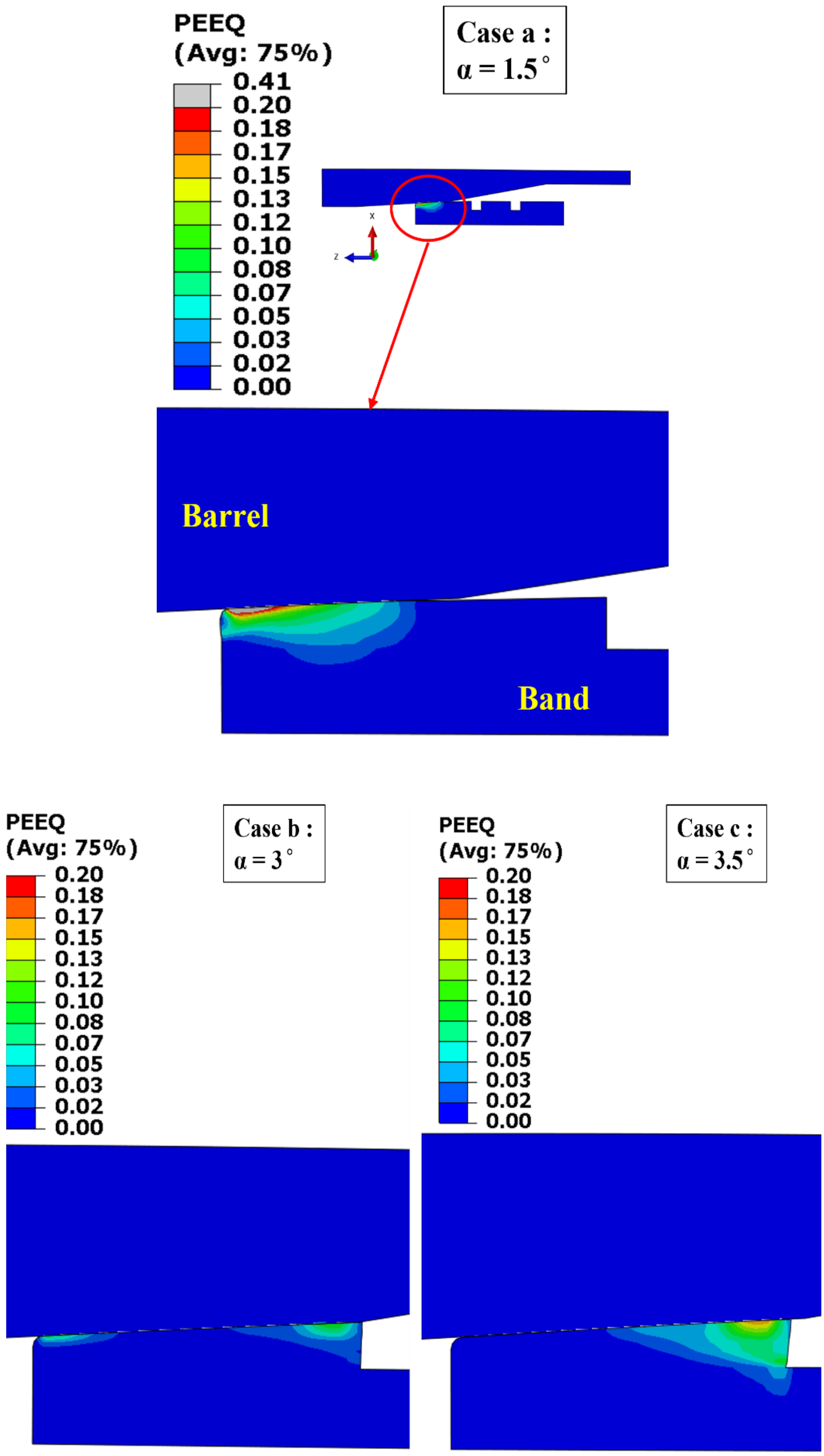


**Fig. 4.12.** Contours of equivalent plastic strain indicating the plastically deformed portion of band for cases a, b and c respectively.

Further, the shape and size of the contact zone can be estimated by observing the contours of contact pressure, CPRESS. **Figs. 4.13 - 4.15** show that the contacting area can be approximated as a rectangle. The dimensions of contact zone on the engraved band are marked for same three cases in **Fig. 4.13 - 4.15.** Maximum contact area is obtained for *case b*, followed by *case c*, whereas least contact area is obtained for *case a*. Note that the angle of forcing cone at the start of rifling is very close to 3$^\circ$. Thus, when $\alpha$ value approaches to three degrees, the forcing cone and upper surface of rotating band become approximately parallel resulting in larger contact area as noticed in *case b.* Thus, contact area being the dominant over contact pressure results in highest contact force for the band with inclination angle of leading surface equal to 3$^\circ$.

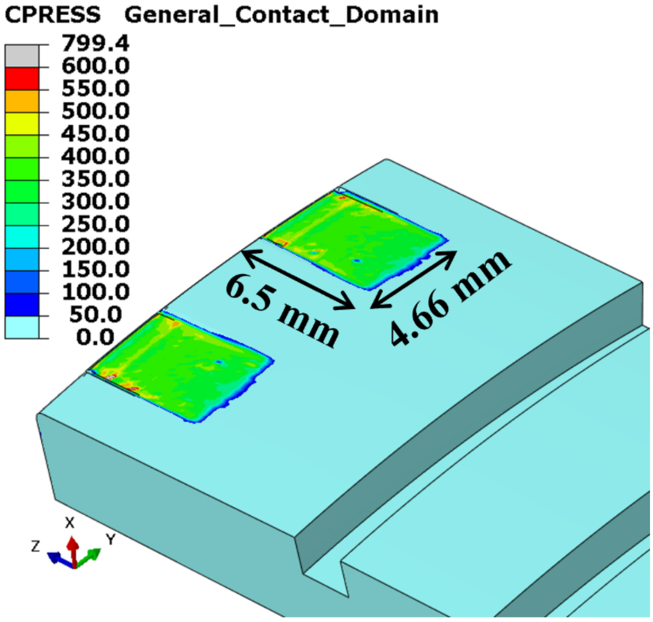


| | |
|---|---|
| **Inclination angle (α)** | **1.5$^\circ$** |
| **Area of contact** | **60.58 mm$^2$** |

**Fig. 4.13.** Engraved profile on the 1.5$^\circ$ inclined band surface

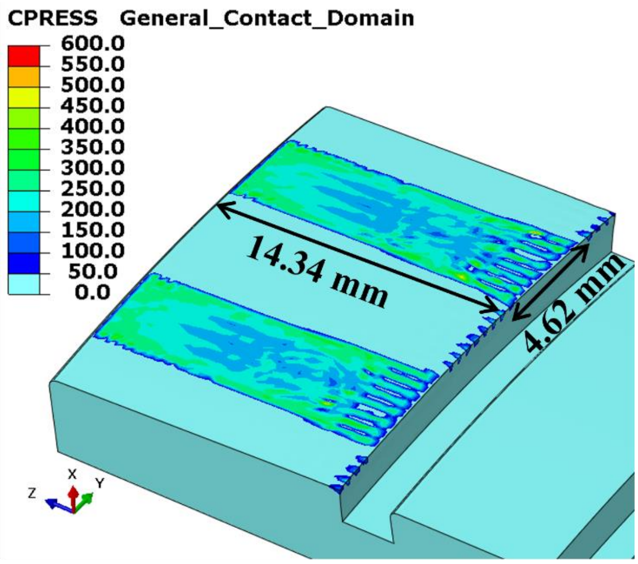


| | |
|---|---|
| **Inclination angle (α)** | **3 °** |
| **Area of contact** | **132.5 mm²** |

**Fig. 4.14.** Engraved profile on the 3 ° inclined band surface

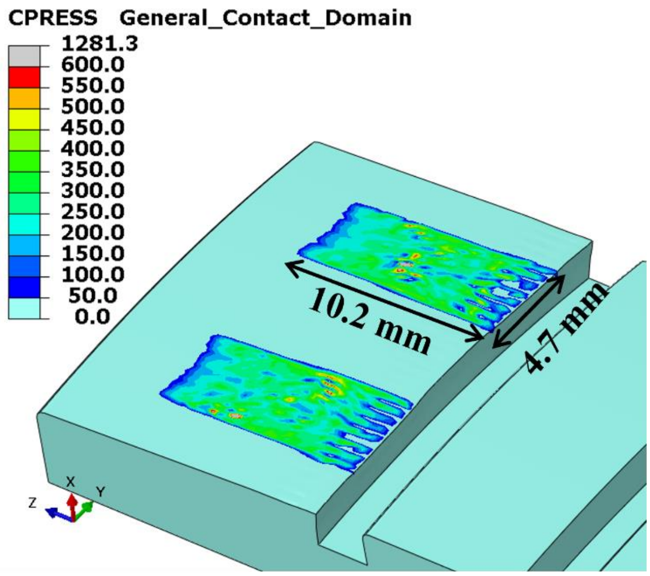


| | |
|---|---|
| **Inclination angle (α)** | **3.5 °** |
| **Area of contact** | **95.88 mm²** |

**Fig. 4.15.** Engraved profile on the 3.5 ° inclined band surface

## Chapter 5

# Finite Element Simulation of Engraving Process

### 5.1 Introduction

The most important function of the artillery gun is to accurately fire the projectile towards the long-range target. To achieve this goal, there is necessity of high muzzle velocity, which can be obtained by developing large propellant gas pressure. But while satisfying all these requirements there is possibility of failure of rotating band as it engraves due to rifling in barrel, and if the band fails during engraving, the performance of gun will be hampered. This demands in-depth investigation of the engraving process. This chapter is completely devoted to the numerical analysis of engraving process. As the engraving process is very rapid, explicit dynamic Finite element simulations are performed, details of which are given in Section 5.2. The results obtained from the simulations are compared with experimental data provided by **ARDE** in Section 5.3.

### 5.2 Details of FE simulation

In chapter 3, the 3D modelling and FE discretization for artillery gun barrel system is already discussed. In this section the application of load and boundary conditions employed in the simulations of engraving process are explained. Due to the burning of propellant, large gas pressure builds up in the barrel chamber. The evolution of chamber pressure in the present gun system is provided by **ARDE**, Pune. This pressure is applied at base of projectile in the simulations of engraving process. **Fig. 5.1.** describes the application of load and boundary condition in the present simulations. For the sake of good visualization, only half section of complete 3D model is shown in

**Fig. 5.1**. All the nodal degrees of freedom are restricted for the one face of barrel which constraints the barrel in one position. The propellant gas pressure is applied on the base of the projectile. **Fig. 5.2** indicates initial positions of components of gun system at the start of engraving.

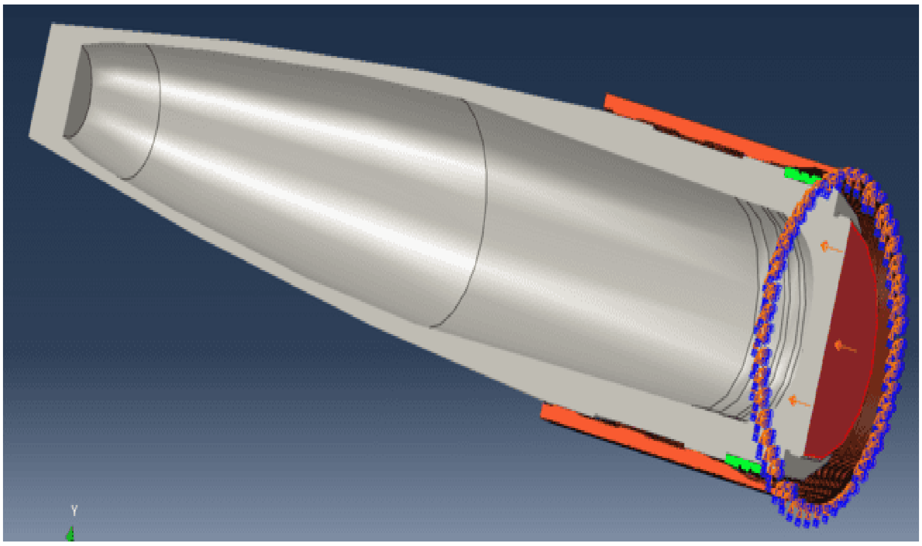

**Fig. 5.1:** Application of load and boundary condition for FE simulation of engraving process.

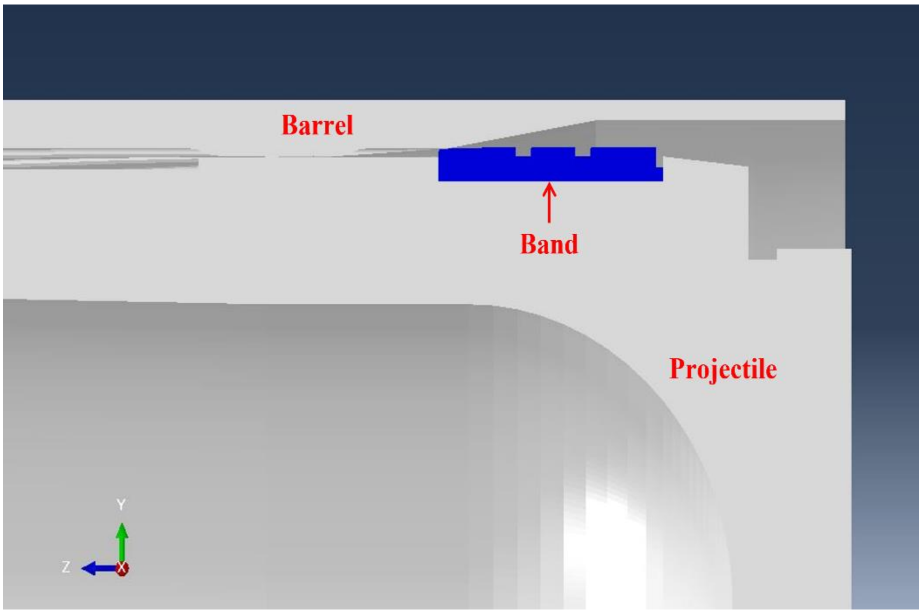


**Fig. 5.2:** Sectional view of gun system at the start of engraving.

## 5.3 Results and discussion

### 5.3.1 Formation of lands and grooves on rotating band

A single step explicit dynamic FE simulation is performed for the analysis of engraving process,. It is observed that the engraving on the entire width of band takes place in just 2.4 milliseconds. **Fig. 5.3** shows the engraved band at this time increment.

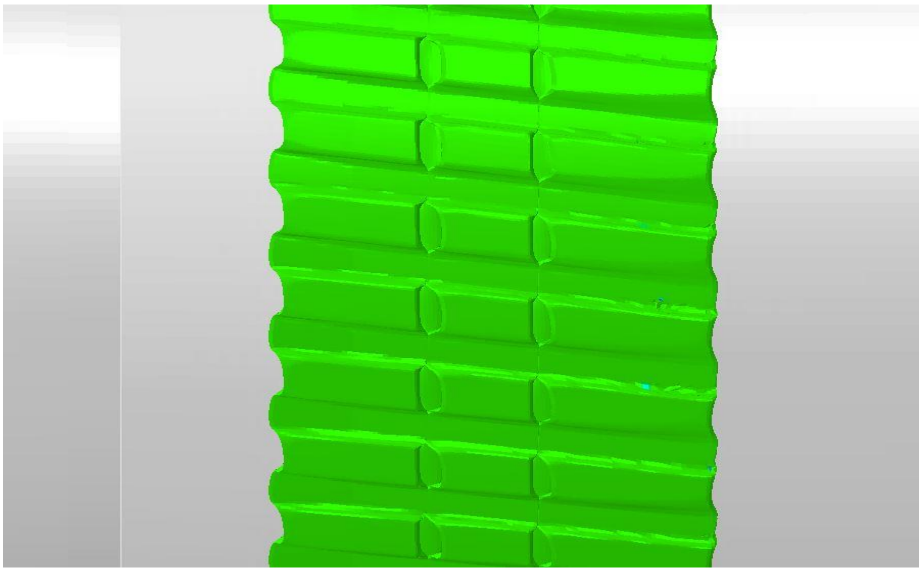

**Fig. 5.3:** Engraved profile of rotating band obtained by simulation.

**Fig. 5.4:** Engraved profile of rotating band provided by ARDE.

On the circumference of the band, two slots are given, known as cannelure, to accommodate the excess material when band is being engraved. From **Fig. 5.3** it can be seen that these cannelures are completely filled with band material in land region, whereas for the band region which is compressed by the grooves in barrel, the cannelures still exist, though severely deformed. **Fig. 5.4** shows the image of a deformed band recovered after firing from the actual gun by **ARDE**. The shapes of deformed band obtained from FE simulations and experiments are quite similar which validates the developed FE model for engraving process.

As the height of rifling in barrel is already known, the second check to ensure correctness of predictions of FE simulation is to measure groove height on the engraved band. **Fig. 5.5** shows that the height of groove in deformed band is 1.258 mm which is very close to the height of 1.27 mm of corresponding grove in the barrel.

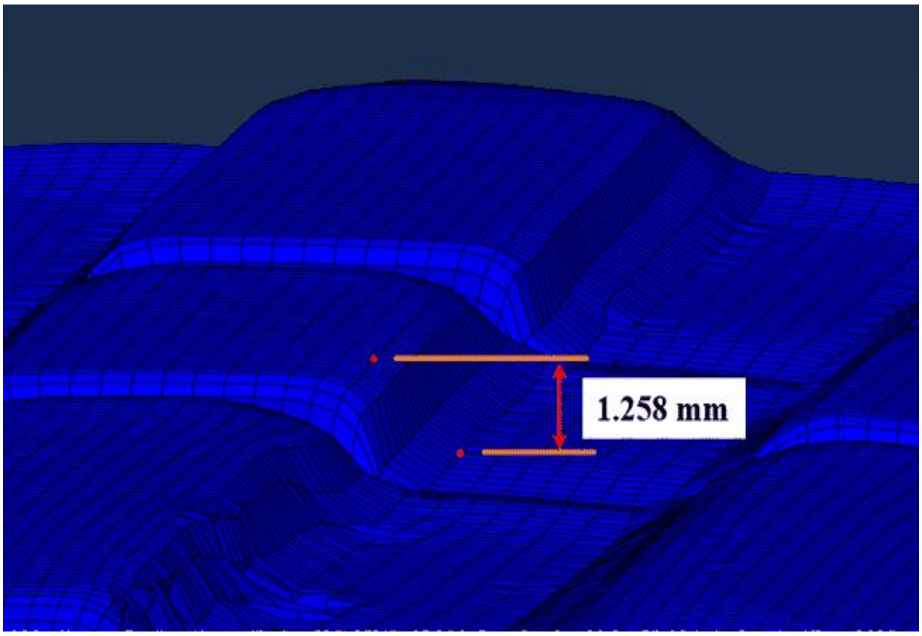


**Fig. 5.5:** Height of the grooves form on the rotating band

During the engraving simulation, some elements deformed heavily. The large distortion of elements demands significant reduction in critical time step for computation. This, in turn, results in, delayed convergence and hence increases in the computation time. To overcome this difficulty, the option of element deletion is enabled. Though this option facilitates rapid computation, the element deletion should be within the limit as there is loss of mass and energy associated with deleted element. The complete model of artillery gun system is discretize by 32,14,560 elements, out of which rotating band consist of highly refined 22,71,360 C3D8R elements. For this simulation 4794 band elements got deleted which is just 0.211% of total elements lying in rotating band.

The contour plots of Von-Mises stress in the rotating band corresponding to the end of engraving process is shown in **Fig. 5.6.** A large stress concentration can be seen on the walls of grooves which are engraved on rotating band. For the remaining region of the band stress values are in the range of 500-600 MPa.

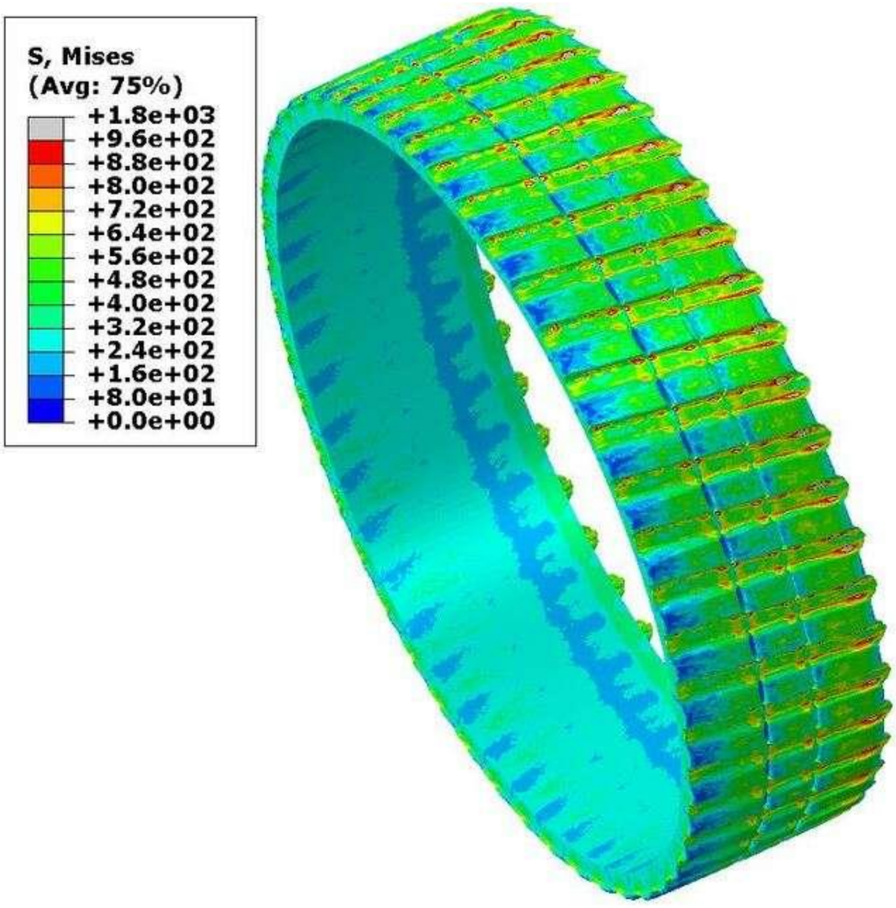


**Fig. 5.6:** Mises stress contour for fully engraved band

### 5.3.2 Evolution of Engraving resistance

As the name suggests, the engraving resistance is the resistance offered by the rotating band during engraving process. It is nothing but resultant force from plastic deformation of band and friction between the contacting surfaces of band and barrel. **Fig. 5.7** depicts the evolution of engraving resistance (**ER**).

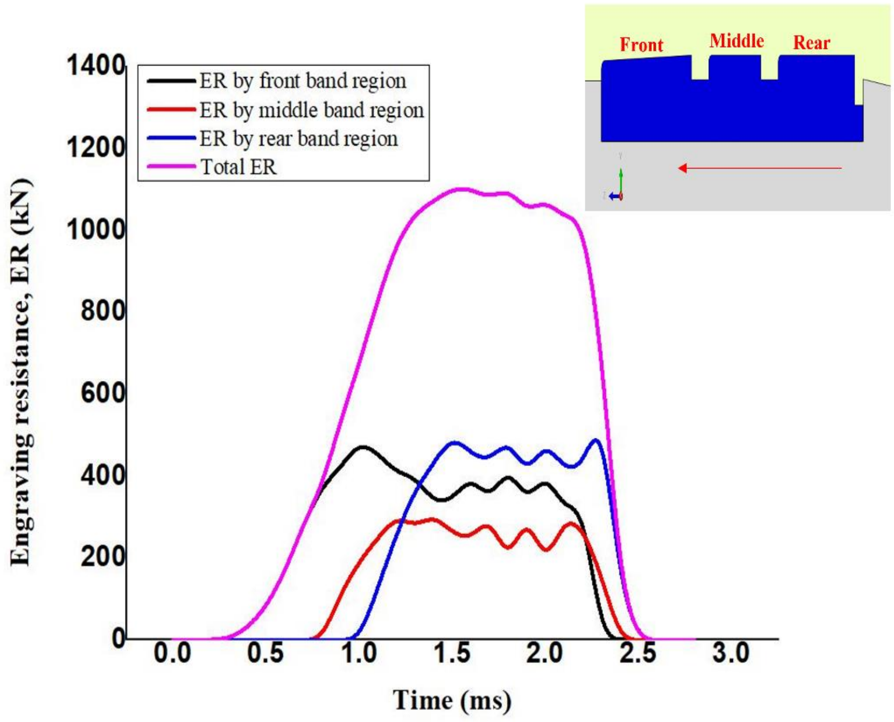


**Fig. 5.7:** Evolution of engraving resistance with time

The rotating band is divided into the three regions due the presence of two cannelure. The black, red, blue color curves in Fig. 5.7 indicate the resistance offered by the front, middle and the rear region of the band, respectively. However, the pink color curve represents the total resistance offered by the band (see Fig. 5.7). It can be observed that the engraving resistance increases as the rotating band gets more deeply engraved and then goes into saturation with small oscillations. Finally, it drops down as the deformation of the rotating band reduces until the rotating band is engraved completely due to the presence of barrel rifling.

The sensitivity of the material towards the strain and strain rate greatly influences the engraving resistance. As the strain rate hardening causes an increase in the yield stress of the rotating band which further increases the deformation resistance of rotating band and thus the engraving resistance. If the propellant gas pressure is more impulsive, band material will undergo deformation with high strain rate and becomes more resistive towards the engraving.

### 5.3.3 Effect of band geometry

As discussed earlier, cannelure present on the circumference of the band accommodates the excess material when band is being engraved, but during this accommodation phenomenon metal to metal contact takes place as shown in **Fig. 5.8.** This acts as a locking for the flow of band material and further resists the engraving of band which increases the engraving resistance.

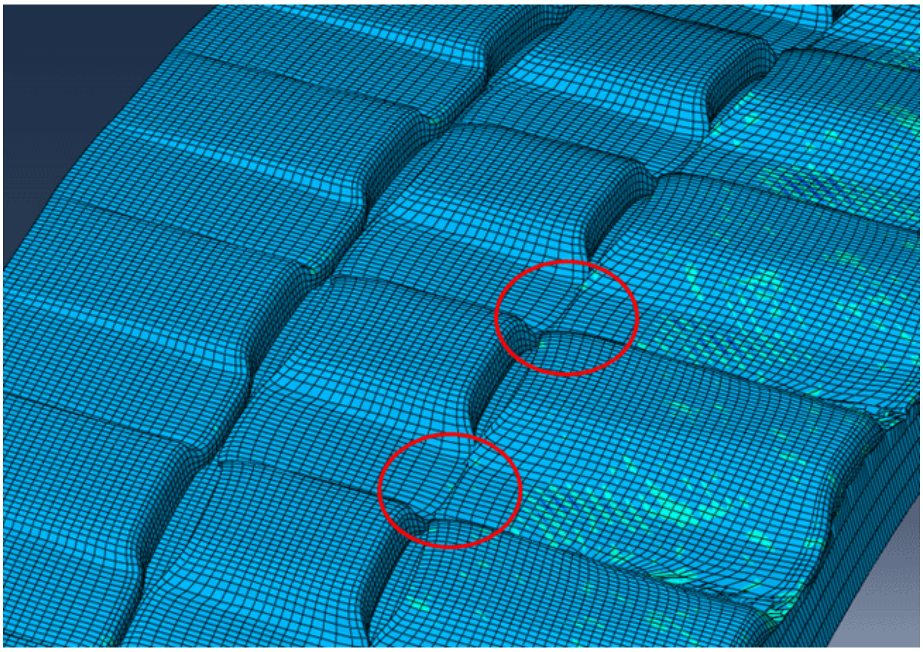

**Fig. 5.8:** Self contact of band material during engraving.

The slight inclination in the vertical surfaces of cannular may help to reduce metal to metal contact and hence engraving resistance. In order to verify this, the geometry of band is modified by providing an inclination of 10 ° on the vertical surfaces of cannular. The sectional view of actual and modified geometry of the rotating band is shown in **Fig. 5.9.**

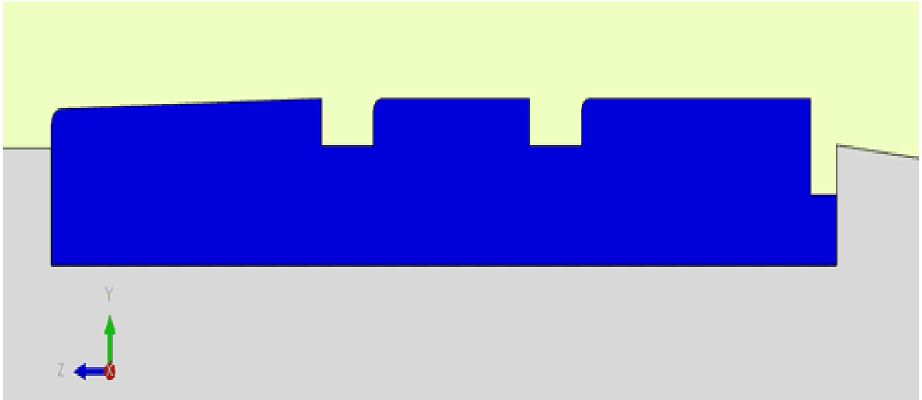

**Fig. 5.9 (a):** Actual band geometry (vertical cannelure)

**Fig. 5.9 (b):** Modified band geometry (10 ° tapered cannelure)

To investigate the effect of band geometry, engraving process is again simulated with modified band geometry while keeping all other conditions same. Results obtained by this simulation are compared with original results. It is observed that the issue of metal-to-metal contact is reduced significantly, which is shown by sectional view of deformed band in **Fig. 5.10.** It can be seen that in actual band, elements present on the opposite walls of cannelure are in contact at the time of engraving whereas, no such new contact formation is observed for the band with modified geometry.

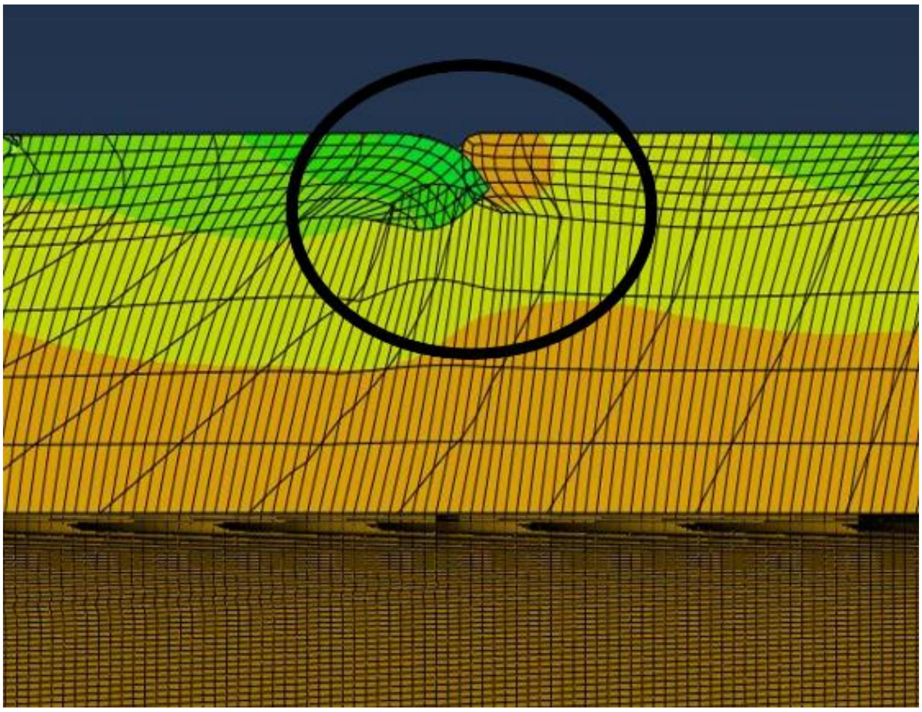

**Fig. 5.10 (a):** Sectional view of engraved band (with vertical cannelure)

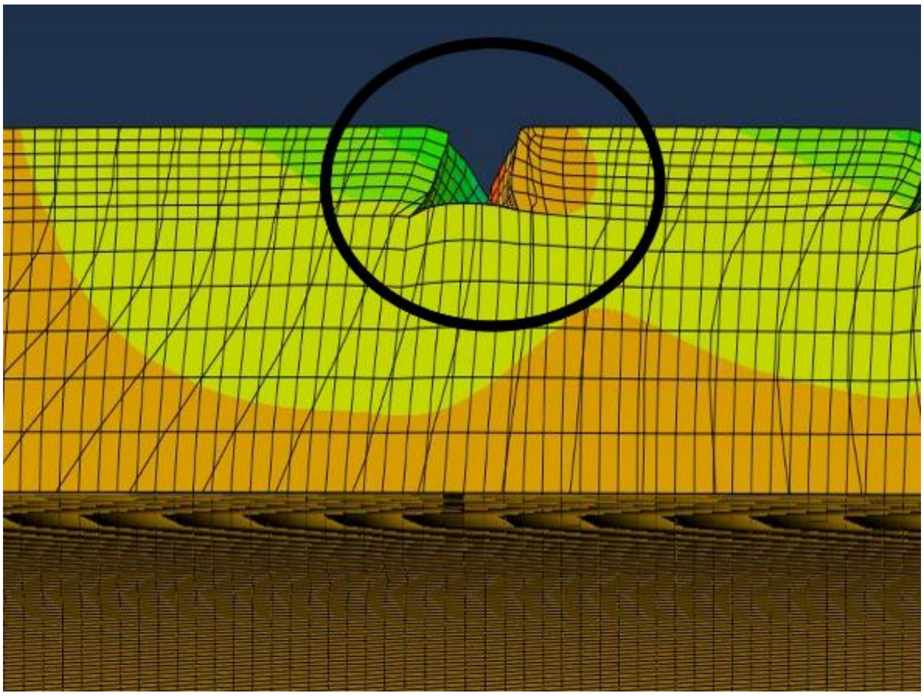

**Fig. 5.10 (b):** Sectional view of engraved band (with 10 ° tapered cannelure)

**Fig. 5.11** depicts that the band with modified geometry has undergone the engraving process much smoother as compared to the actual band. There is no peculiar deformation of any element and nice engraved profile is obtained. As the extreme distortion of rotating band is minimized, it suggests that chance of failure of rotating band during engraving process is also reduced with this modification,

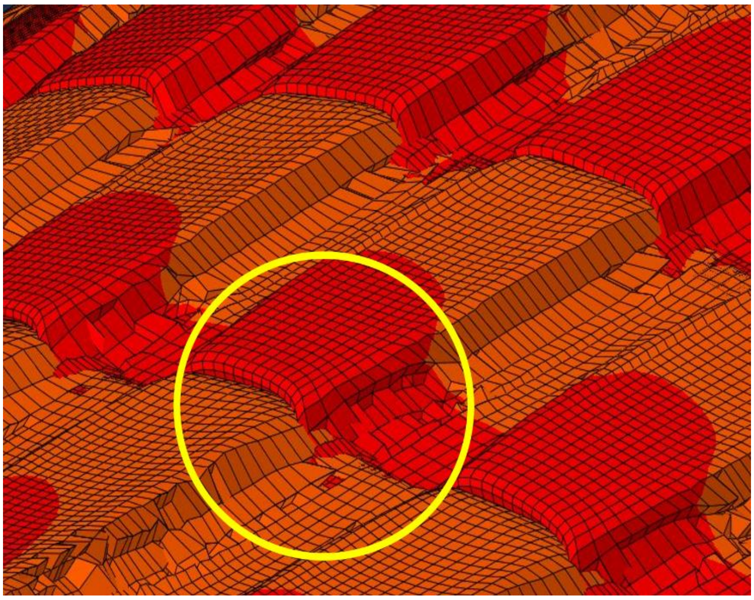

**Fig. 5.11 (a):** Engraved profile of rotating band with vertical cannelure

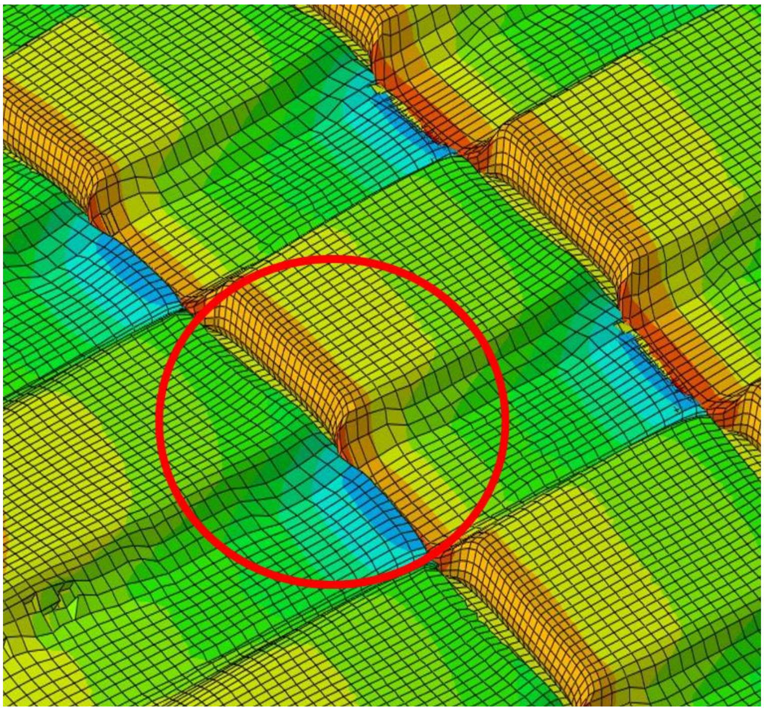

**Fig. 5.11 (b):** Engraved profile of rotating band with tapered cannelure

## Chapter 6

# Conclusion and Future Scope

### 6.1 Introduction

In this work, ramming and engraving operation particularly for gun barrel with 155 mm bore has been analyzed by performing explicit dynamic finite element simulations. The effects of some important factors which influence these operations, such as barrel wear and rotating band geometry, are examined in order to fulfill the stated objectives. The important conclusions from the present work and the future scope of study are summarized in Sections 6.2 and 6.3 respectively.

### 6.2 Conclusions

Important conclusions from this work are as follows.

- The retention force established as a result of interaction between rotating band and barrel inner surface is highly influenced by initial ramming velocity.
- To satisfy the fallback prevention criteria and to have proper ballistic performance even with barrel having wear within specified limit, it is necessary to position the projectile with high ramming velocity depending on severity.
- As the wear of barrel increases, projectile needs to travel more for establishment of contact, this causes increase in chamber volume of barrel and thus affects the development of propellant gas pressure.
- The inclination angle of leading surface of band is the important parameter in the band geometry which decides the extent of plastic deformation in band. As this angle approaches

the forcing cone angle of barrel (here it is $3^{\circ}$), maximum contact force is generated, which is desired condition for effective ramming operation.

- By tapering the cannelure of rotating band, difficulty of metal-to-metal contact in engraving process can be solved and much smooth engraved profile of band is obtained, This reduces the failure chances of rotating band.

## 6.3 Future Scope

Although the suggested numerical approach is effective and in accordance with the experimental results, a few concerns need to be addressed for more accuracy. Future research efforts might be focused on the following areas:

- The engraving process can be further studied by considering the combined effects of the combustion of propellant and the mechanical interactions.

The thermal effect and the influence of material properties of rotating band on both, ramming and engraving process, can be analyzed by changing the material of rotating band.

# REFERENCES


[1] Ding, Chuanjun, Ning Liu, and Xiangyan Zhang. "A mesh generation method for worn gun barrel and its application in projectile-barrel interaction analysis." Finite Elements in Analysis and Design 124 (2017): 22-32.

[2] Chao-bin Hu, Xiao-bing Zhang, Influence of multiple structural parameters on interior ballistics based on orthogonal test methods, School of Energy and Power Engineering, Nanjing University of Science and Technology, China,2019.

[3] Zhen li, Jianli Ge, Modeling and dynamic simulation on engraving process of rotating band into rifled barrel using three different numerical method, Journal of Vibroengineering,2016

[4] J. Balla, R. Jankovych and V. Y. Duong, Interaction between projectile driving band and forcing cone of weapon barrel, (Published Conference Proceedings style), Nov 2011.

[5] J. N. Kriel & De Malan, Measuring some Parameters Relevant to the ballistic Performance of a 155mm Gun System, (Published Conference Proceedings style). Somchem, a Division of Denel (Pty) Ltd. South Africa. In: Proceedings of IIIrd European Guns, Mortars and Ammunition Symposium. Shrivenham: RMCS, UK, SEPT 1996.

[6] H. A. Liechti, Ammunition Feeding for Large Calibre Guns, (Published Conference Proceedings style). In: The Proceedings of IVth European guns and ammunition symposium, Shrivenham: RMCS, UK, SEPT 1997, pp. 1-34.

[7] J. Balla, "Dynamics of Mounted Automatic Cannon on Track Vehicle (Periodical style)", In International Journal of Mathematical Models and Methods in Applied Sciences). NAUN press, December 2011, pp. 423-432. ISSN 1998-0140.

[8] J. Balla, V. Y. Duong, “Analysis of feeding device with two degrees of freedom (Periodical style)”, In International Journal of Mechanics. NAUN press, 2011, pp. 361-370. ISSN 1998-4448.

[9] H. A. Liechti, Ammunition Feeding for Large Calibre Guns, (Published Conference Proceedings style). In: The Proceedings of IVth European guns and ammunition symposium, Shrivenham: RMCS, UK, SEPT 1997, pp. 1-34.

[10] Large Calibre Ordnance/Munition Compatibility, Design SafetyRequirements and Safety and Suitability for Service Evaluation COS 109002 Czech Defence Standard. Prague: MoD, 2005.

[11] J. Balla, V. Y. Duong., Jankovych. R., Evaluation of 152 mm SPH M77 ramming device. (Published Conference Proceedings style),” In Proceedings from International Conference on Military Technologies. Brno University of Defence, 2011, ISBN 978-80-7231-787-5, pp. 1625- 1634.

[12] J. Balla, V. Y. Duong, R. Jankovych, Technical Inspection of 125 mm tank cannon ramming device. (Published Conference Proceedings style),” In The Proceedings from International Conference on Military Technologies. Brno: University of Defence, 2011, ISBN 978-80-7231-787-5, pp. 1635-1644.

[13] J. Balla, R. Jankovych, V. Y. Duong, “Procedure of Extraction Force Measuring from the 152mm barrel . (Published Conference Proceedings style),” in The Proceedings from International Conference ICMT´10 - International Conference on Military Technologies. Bratislava, Slovakia, 2010. ISBN 978-80-8075-454-9.

[14] J. Balla, Stanislav Prochazka, Van Yen Duong, Evaluation of projectile ramming process in new and worn smooth barrels of guns, International Journal of Mechanics (2013)

[15] S. Procházka, N. D. Ninh, Differences in Barrel Chamber and Muzzle Deformation during Shot (Periodical style – Accepted for

publication),” Advances in Military Technology, ISSN 1802-2308, to be published. Brno University of Defence, 2011, ISBN 978-80-7231-787-5, pp. 1785- 1792.

[16] Heyang SUN, Jisheng MA, Longbo SHENG, Wei LI, Dalin WU, CDM Model and its Application to Numerical Simulation on Rotating Band’s Engraving Process, China naval flying academy, 2015

[17] Andrews TD. Projectile driving band interactions with gun barrels. J Press Vessel Technol 2006;128:273e8.

[18] Quanzhao Sun, Guolai Yang and Jianli Ge (2015), “Modeling and simulation on engraving process of projectile rotating band under different charge cases”, Journal of Vibration and Control.

[19] Abaqus 2017, Theory manuals, Version 6.5. Hibbit, Karlsson and Soresen Inc., RI, USA.

[20] R. Jankovych, Tube weapons and ammunition (Book style). Brno, University of Technology, ISBN 978-80-260-2384-5, pp. 128.